universität wien

MASTERARBEIT | MASTER'S THESIS

Titel | Title

Investigation of polydisperse F8BT–labelled PET and PP nanoplastic suspensions and the mass-based quantification of cellular uptake

verfasst von | submitted by

Patrick Wrightman Treacy

angestrebter akademischer Grad | in partial fulfilment of the requirements for the degree of

Master of Science (MSc)

Wien | Vienna, 2024

Studienkennzahl lt. Studienblatt | Degree programme code as it appears on the student record sheet:	UA 066 606
Studienrichtung lt. Studienblatt | Degree programme as it appears on the student record sheet:	Masterstudium Drug Discovery and Development
Betreut von | Supervisor:	Univ.-Prof. Dr. Lea Ann Dailey

Acknowledgements

I would like to express my sincere gratitude to my advisor, Univ.-Prof. Dr. Lea Ann Dailey, for giving me the opportunity to work in her research group. Her guidance and support were invaluable for the completion of this project.

A special thank you goes to Mag. My Vanessa Nguyen Hoang, for teaching me the intricacies of cell culture techniques and guiding me with the theoretical and practical aspects of this research, and to Mag. Lukas Wimmer, Sandy Adel, and Johannes Szilvassy for their valuable instruction and assistance in the production of nanoplastic suspensions. I would also like to express my appreciation to the entire lab for fostering a welcoming and productive atmosphere, conducive to academic growth and collaboration.

My partner, Anna, deserves my admiration for inspiring optimism in both blissful and trying times. Lastly, I would like to extend a heartfelt thank you to my parents, Pat and Ellen, for the support and the freedom they provided me along the way.

Disclaimer

To aid in the writing of this manuscript, ChatGPT version 3.5 was used in some sections of this document to generate small sections of text, which were then edited by the author. Grammarly was used to spellcheck and edit the document.

Table of Contents

Abstract

Plastic particles have been detected in the environment worldwide and more recently, smaller particles known as nanoplastics have been identified in air samples, reaching as far as remote alpine environments. The impact of nanoplastics on human health remains unclear, necessitating further research to understand their potential toxicological effects and implications for human exposure. Nanoplastics are often nonhomogeneous and vary in size, surface chemistry, and structure. This affects dosimetry, often leading to a lack of reproducibility between studies and misrepresented dosage values. To better understand the biological impact of nanoplastics, more reliable reference materials must be produced in addition to improving detection techniques. In this study, Poly(9,9-dioctylfluorene-alt-benzothiadiazole) (F8BT)-labelled polypropylene (PP) and polyethylene terephthalate (PET) fluorescent nanoparticles with different percentages of dye loading (0.8% and 5%) were prepared by nanoprecipitation and the size distributions were measured by static light scattering (SLS). PP–F8BT (0.8%) and PET–F8BT (0.8%) batches were produced in the 0.1 – 1 μm range, but aggregation led to large particle formation. The limit of detection (LOD) of PET–F8BT (0.8%) was 5- to 10-fold lower compared to PP–F8BT (0.8%) depending on the medium used. Theoretical delivered dose values were calculated by two computational methods, *in vitro* Sedimentation, Diffusion, and Dosimetry (ISDD) and RiskGone *in vitro* Dosimetry. Based on the predicted concentrations by the computational models, Calu-3 human lung epithelial cells were treated with PP–F8BT (5%) and PET–F8BT (5%) glycerol suspensions, and the cellular uptake was assessed by mass-based fluorescence detection. The cellular dose was measured for PET–F8BT (5%) at 250 μg/mL = 1.38 ± 0.7 μg/cm^2 and 500 μg/mL = 2.84 ± 1.1 μg/cm^2, but the background signal was nearly as high. PP had no measurable uptake.

List of Abbreviations

Abbreviation	Definition
AD	Administered Dose
CD	Cellular Dose
CO_2	Carbon Dioxide
CPN	Conjugated Polymer Nanoparticles
DD	Delivered Dose
DG	Distorted Grid
DMSO	Dimethyl Sulfoxide
F8BT	Poly(9,9-dioctylfluorene-alt-benzothiadiazole)
FTIR	Fourier Transform Infrared
H_2O	Water
IC50	Inhibitory Concentration 50%
IFN-γ	Interferon-gamma
IL-12	Interleukin-12
ISDD	*In vitro* Sedimentation, Diffusion, and Dosimetry
ISO	International Organization for Standardization
LOD	Limit of Detection
LOQ	Limit of Quantification
MNPs	Micro- and nano-plastics
MTT	3-(4,5-dimethylthiazol-2-yl)-2,5-diphenyltetrazolium bromide
NIPS	Nonsolvent Induced Phase Separation
OLED	Organic Light Emitting Diode

PBS	Dulbecco’s Phosphate Buffered Saline
PE	Polyethylene
PET	Polyethylene terephthalate
PM2.5	Particulate Matter 2.5
PMA	Phorbol-12-myristate-13-acetate
PP	Polypropylene
PS	Polystyrene
PUR	Polyurethane
PVC	Polyvinyl Chloride
RB	Round Bottom
ROS	Reactive Oxygen Species
RPM	Rotations per Minute
RSD	Relative Standard Deviation
SEM	Scanning Electron Microscopy
SLS	Static Light Scattering
TNFα	Tumor Necrosis Factor-alpha
Tw80	Tween®80
UV	Ultraviolet

1. Introduction

1.1. Plastics Background

Nowadays, the use of plastics is widely spread, and they constitute a significant portion of consumer goods worldwide. Plastics are synthetic, carbon-based compounds made up of linked polymer chains. [1] The chemical structure of individual monomers defines different types of plastics, with strong covalent bonds linking individual monomer units. These chemical characteristics are highly desirable in global economy, with low permeability, high strength and flexibility, low weight, and low cost of production leading to economic dependence on these materials. The most common types of plastics are thermoplastics, including polyethylene (PE), polypropylene (PP), polyvinylchloride (PVC), polyethylene terephthalate (PET), polyurethane (PUR), and polystyrene (PS). For instance, PP accounts for 21% and PET less than 10% of the total plastic production. [2]

While plastics present benefits in terms of convenience and cost, persistence and overuse have led to high levels of pollution. It is estimated that a gross of approximately 8.3 billion metric tons of plastics have been produced until 2015, with increasing production rates and persistently low recycling rates. [2] Plastics have incredibly long lifecycles once they enter the environment, and subsequently, there is an ever-growing pressure on individuals, governments, and producers to reduce, reuse, and recycle plastics to manage the environmental crisis. Single-use plastics and plastic packaging are dominant contributors to the overall plastic fraction, as evidenced by ever increasing portion of total global waste. [3] A vast majority of commonly used plastics do not biodegrade, and therefore accumulate in landfills and the environment. [4] Nano- and micro-sized plastics enter the environment either as primary pollutants, where small plastic particles are intentionally manufactured in consumer products such as cosmetics [5], or as secondary pollutants, which arise from the degradation of larger plastic goods. Breakdown pathways for plastics include ultraviolet (UV) degradation, mechanical abrasion, and chemical decomposition. [6] Plastics migrate to waterways and eventually oceans, where harsh conditions cause degradation significantly faster than on land. [1] Detection of microplastics in alpine glaciers provided evidence that MNPs are aerosolized and eventually deposited by precipitation in even the most remote environments. [5]

Microplastics are almost universally cited with an upper size limit of 5 mm. [7] On the other hand, the lower limit is opined to be as low as 1 μm, or as high as 1 mm. [7,8] The justification for debate on the definition stems from collection and detection limitations, as well as the environmental and biological fate of different particle sizes. The upper size limit for nanoplastics is claimed to be either 100 nm or 1000 nm. [8] The International Organization for Standardization (ISO) defines nanoplastics within a range of 1 nm – 1 μm, with ISO specifically categorizing them as "plastic particles smaller than 1 μm". [9] Furthermore, Gigault, *et al.* (2018) argued that the colloidal behavior exhibited by particles between 1 nm – 1 μm should define the term “nanoplastics”. [10] Consequently, this study will refer to nanoplastics according to the ISO definition. Micro- and nanoplastics (MNPs) is a term that encompasses both classes, stemming from the fact that medical and environmental studies report the detection of a wide range of plastic sizes. [11,12]

1.2. Impact on Human Health

Ingestion and inhalation are the main pathways through which MNPs can enter the human body [13], with inhalation being a primary concern. While the health implications of inhaled MNPs are not fully understood, they are surmised to induce inflammatory responses associated with conditions such as asthma. [13] Furthermore, microplastic particles have been recorded in lower-lung tissue samples, with PP and PET being the most abundant. Micro Fourier Transform Infrared (μFTIR) spectroscopy confirmed the identity of particles ≥ 3 μm. [14] While confirming that plastics are indeed inhaled, the method does not account for nano-sized plastics. Studies on particulate matter smaller than 2.5 μm in diameter (PM2.5) have been correlated with increased human mortality. [15] PM2.5 induced expression of cytokines interleukin-12 (IL-12) and interferon-gamma (IFN-γ) in M1 alveolar macrophages, associated with an increased inflammatory response. [16] While PM2.5 is an unspecific particle measure, consisting of a wide range of pollutants, PS nanoplastics have been shown to increase inflammatory cytokines and internalize in human alveolar cells. [17] PM2.5 can penetrate deep into lung alveoli and reach endothelial cells, indicating particles of this size can reach the lung endothelium. [16]

PP nanoparticles with a diameter of 0.66 ± 0.27 μm induced inflammation and reactive oxygen species (ROS) formation in the lungs when administered to mice at high

doses. [18] However, it is important to note that the doses used in this study are orders of magnitude higher than that which humans would likely be exposed to, based on the finding that urban air contained PM2.5 plastics at concentrations of around 238 ng/m^3. [19]

While these studies suggest that plastic particles can have negative health effects, the choice of reference plastic material used in such studies warrants closer scrutiny. From the studies cited above, there are several different plastic types, sources (e.g. from reference material, biological tissue, or the environment) and sizes of plastic, often reported as a single diameter. Even though the studies listed above fall under the term MNPs, it becomes difficult to identify common threads which could single out specifically which qualities of MNPs could harm human health. Scientists have identified this lack of cohesion within the MNP field as a source of disjointedness, stemming from inconsistent reporting of particle size, concentration, identity, shape and plastic source, among other criteria. [20,21] A significant issue that has often been overlooked is the lack of standardized, uniform reference materials, which can introduce variability in experimental results. This convolutes the interpretation of particle toxicity and biological impact, as the differences in physical and chemical particle characteristics are not accounted for. There is an underscored need for high-quality, well-characterized reference materials to ensure reproducibility and accuracy in dosimetry-based nanoplastic studies. [22] The absence of such standardized materials compromises the comparability of results across different studies, limiting the broader applicability of findings on nanoplastic particle toxicity.

1.3. *In Vitro* Dosimetry

Particle dosimetry can begin to explain the core concepts which underline why particles need to be treated differently than classic pharmacological molecules. One core principle in pharmacology is that when a target is influenced by a compound–whether a molecule or a particle–it produces a measurable response. This response is more strongly correlated with the dose at the target site than with the dose initially administered. In *in vitro* cell culture studies, three key doses are often referenced. The **administered dose** (or nominal dose) refers to the amount of compound initially given to a subject. The **delivered dose** is the amount that reaches the target tissue and deposits onto the cell monolayer but does not necessarily cross the cellular membrane. Finally, the **cellular**

dose is the amount that interacts with and is internalized by the cells. [23–25] **Figure 1** illustrates these concepts, showing particles (represented by dark blue circles) in a well

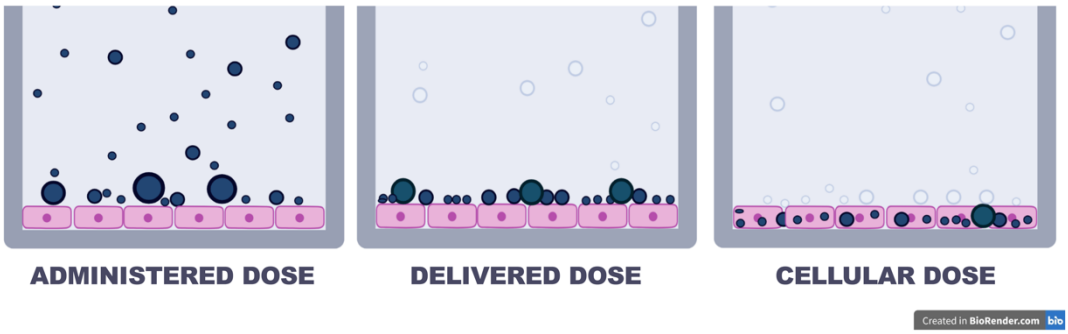

Figure 1. Visual depiction of the administered dose (left), delivered dose (middle), and cellular dose (right). Created in BioRender.

plate, where the pink layer at the bottom symbolizes a monolayer of adherent cells.

Teeguarden *et al.* (2007) highlighted the need for rigorous standards in particle dosimetry, stressing that it differs fundamentally from chemical dosimetry. While chemicals are generally solubilized in biological media, particles remain as colloids, suspended amongst the medium. This distinction significantly impacts how dosimetry metrics are calculated. For chemicals, mass or concentration-based measurements are typically sufficient, but for particles, especially at the nanoscale, metrics such as surface area and particle number offer a more accurate description of exposure. [23,26] Since particles are often much larger and fewer in number compared to small molecules, using these alternative metrics is crucial for a proper understanding of nanoparticle behavior and interaction with biological systems.

The challenge of comparing administered doses across different biological models further emphasizes the need for standardized particle dosimetry approaches. Anatomical variations between animal models and humans can result in significant differences in how particles deposit, are taken up and elicit biological responses. Differences in organ size, blood flow, and tissue architecture contribute to this variation. Teeguarden, *et. al.* (2007) demonstrated that using biological dosimetry metrics, like normalizing to the target tissue surface area, led to more comparable results across species. [27,28] These metrics provide a better framework for understanding particle behavior in biological systems by accounting for the anatomical differences between species.

Another critical factor influencing dosimetry is the size and density of the particles. These characteristics determine how particles deposit onto cellular surfaces. Larger and

denser particles sediment more quickly and are more likely to deposit than smaller or less dense particles, influencing how they interact with cells. [23,29] Additionally, cellular uptake mechanisms vary based on particle size and cell type. For example, PS nanoparticles smaller than 20 nm are primarily internalized by passive diffusion in macrophages, while larger particles, around 500 nm, are taken up through active endocytosis processes, such as phagocytosis or receptor-mediated endocytosis. [30] This variation underscores the importance of considering particle size, shape, and surface properties when assessing nanoparticle-cell interactions.

Nanoparticles also have the potential to develop a biomolecular corona, a layer of proteins and lipids that adheres to their surface in biological fluids. This corona can alter the particles' signalling pathways, uptake, and overall biological fate. The presence of this corona influences biodistribution, aggregation, and the biological response to the nanoparticles. [31–33]

The necessity for robust and consistent dosimetry protocols becomes even more apparent when translating findings from *in vitro* to *in vivo* models or from animal studies to human applications. Without standardized particle dosimetry, the interpretation of nanoparticle health effects or therapeutic efficacy becomes inconsistent and unreliable. The development of standardized reference materials and dosimetry protocols will address these challenges by prioritizing consistency in particle size, dispersity and aim to limit factors like aggregation, which negatively affect cell culture studies.

Based on the need for a predictive tool to calculate deposition rates for small particles, Hinderleiter *et. al.* (2010) created *In vitro* Sedimentation, Diffusion, and Dosimetry (ISDD), which solves a differential equation for particle concentration with respect to time. It is composed of the Stokes-Einstein equation for diffusion and Stokes law for sedimentation to predict the fraction of particles deposited.

$$Modified\ Stokes\ Law\text{: V} = \frac{g(d^2)(\rho_p - \rho_m)}{18\eta} \quad (1)$$

$$Modified\ Stokes - Einstein\text{: } D = \frac{\mathrm{R}T}{3\pi\eta \mathrm{d}} \quad (2)$$

$$\mathrm{d} = particle\ diameter;\ \rho_m = density(medium); \rho_p = density(particle)$$

$$\eta = viscosity(medium);\ T = temperature;\ R = ideal\ gas\ constant$$

$$V = sedimentation\,rate;\ \mathrm{D} = diffusion\,coefficient$$

This model assumes two primary driving forces for particle motion: Sedimentation, driven by gravitational forces, is accounted for by Stokes law. Diffusion is modeled by the Stokes-Einstein equation. These expressions are used to solve the Mason-Weaver partial differential equation [34]:

$$\frac{\partial n}{\partial t} = D\frac{\partial^2 n}{\partial x^2} - V\frac{\partial n}{\partial x} \tag{3}$$

$$x = distance;\ \mathrm{t} = time; n = concentration$$

Particle motion is driven by Brownian motion for smaller diameters, and gravitation for larger diameters. Hinterleiter, *et.al.* (2010) explained the impact of this to be very fast deposition for the largest and smallest particles, and the slowest deposition rate for mid-sized colloidal particles. [35]

Harvard distorted grid (DG) was developed as an improvement of the ISDD model and relies on the same principles of Stokes law and the Stokes–Einstein equation, but DG numerically solves for the concentration of particles in *n* cross sections by tracking the particles when they cross *n+1* boundaries. The result was more computationally expensive but made possible several major features. First, it can analyze a continuous polydisperse sample, whereas ISDD could only compute a single particle diameter. Additionally, particles were treated continuously in the solution, meaning that they could travel up or down the column, resulting in the ability to measure buoyant particles. [29,36]

1.4. Production of MNPs

PS has dominated the MNP research field during the surging public interest in nanoplastics, with 58% of microplastic studies and 91% of nanoplastics performing experiments using PS. [20,37] Two prominent plastics types, PET and PP, are underrepresented in the scientific literature despite being some of the most commonly produced plastics. [20,22] One reason for the lack of studies focusing on these plastics is the lack of a suitable reference material. PP and PET were selected as nanoparticle reference materials due to their prevalence in environmental pollution and their underrepresentation in nanoplastic research. [2,20] PP and PET also exhibit distinct physical and chemical characteristics, making them appealing for comparative studies. PP

is less dense (0.9 g/cm3) than aqueous medium and highly hydrophobic [38], with a simple carbon backbone, while PET has a higher density (1.38 g/cm^3) [39] and contains ester groups, which can participate in hydrogen bonding making in less hydrophobic. These differences influence their behavior in aqueous environments and their interactions with biological systems, making them interesting candidates for studying the environmental and biological impact of nanoplastics.

In addition to the need for reference material, a water-soluble suspension medium non-cytotoxic for *in vitro* and *in vivo* experiments was sought after. Cells cannot be exposed to a typical suspension mediums like ethanol [40], and water does not suspend many nanoplastics for long periods of time. [41] Glycerol was identified as a suitable gold nanoparticle suspension medium, with its high viscosity responsible for stabilizing the nanoparticles for long periods of time. [42] Previous work in the Dailey laboratory found that glycerol was able to suspend nanoplastics and therefore was used as the suspension medium in this study.

Lee, *et.al* (2022) reported PP nanoparticles dispersed in ethanol by high-yield nonsolvent-induced phase separation (NIPS). Size measurement by scanning electron microscopy (SEM) determined a size range of 562.15 ± 118.47 nm. [43] NIPS induces precipitation by mixing two solvents, one in which the polymer is soluble and the other in which the polymer is insoluble. As the dissolved polymer is introduced to the nonsolvent, there is a gradient in chemical potential and the solvent is exchanged, resulting in the precipitation of the polymer. This method has been used to develop porous polymer films [44], but changes in the ratio of nonsolvent to solvent, the rate of mixing, as well as the miscibility of the nonsolvent and solvent impact the structure of the precipitated polymer leading to nanosphere formation. [45,46] NIPS has been used to recycle PET by benzyl alcohol/methanol precipitation, which resulted in high yields and structural similarity. [47] Recently, PET nanoparticles have been prepared via NIPS and labelled using nile red and rhodamine B. [48,49] Nanoprecipitation describes a similar method which has been used to coprecipitate polymer dyes with solvated plastics to produce fluorescent nanoplastics. [50] Another key aspect of nanoplastic production is the fluorescent label, which is needed to distinguish the particles from biological components present in cell culture.

1.4.1. F8BT Fluorescent Label

Since nanoplastics are not easily detected in biological systems, a reliable detection method is needed to confirm their presence. Several techniques exist, including direct observation methods (e.g., microscopy), spectroscopic methods (e.g., light scattering or Raman spectroscopy), and fluorescence-based methods. Limitations of detection methods are dependent on the size of the nanoparticles, the low concentration in which nanoplastics are often present, and interference by biological material. [51]

The yellow-green fluorescent dye poly(9,9-dioctylfluorene-alt-benzothiadiazole), known as F8BT, was first used as an organic light-emitting diode (OLED) but has since been widely used as a model fluorescent label. [32,52–54] The core unit of F8BT is a copolymer of 9-9-dioctylfluorene and benzothiadiazole **(Figure 2).** F8BT possesses a

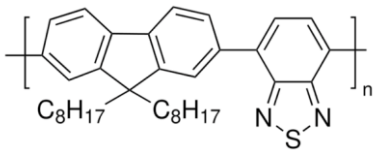

Figure 2. Structure of monomeric unit of F8BT. 9,9-dioctylfluorene (F8) unit is on the left side, and the benzothiadiazole (BT) is on the right.

conjugated π electronic structure, and this high electron mobility is responsible for F8BT's fluorescence. [52] An important metric for fluorescence labels is quantum yield, which is the relationship between the light energy emitted by a fluorophore compared to the amount absorbed. [55] Sensitive fluorophores are much more easily detected *in vitro* and necessary in experiments where small amounts of particles are being measured. F8BT is known to have high quantum yields, defined by the ratio of photons emitted to photons absorbed. [56,57] This characteristic has been demonstrated in conjugated polymer nanoparticles (CPNs) prepared by solvent displacement. [32] Fluorescent polymer dyes are increasingly used for *in vitro* and *in vivo* imaging due to their enhanced photostability and reduced leaching when embedded in polymer nanoparticles. [58] These characteristics arise from the conjugated electronic structure of the polymer and strong hydrophobic interactions with the host plastic matrix. [59,60] The high quantum yield, photostability and polymeric structure of F8BT make it an ideal dye to label nanoplastics with.

1.4.2. Cell Culture Models

In addition to a sensitive dye, an established method which is sensitive to low uptake values is necessary for nanoparticle uptake studies. The first cell culture model chosen was the Calu-3 cell line, which was derived from a human lung adenocarcinoma in the 1970s and is now a widely used model for studying respiratory epithelium. Originating from bronchial submucosal glands and retaining many characteristics of airway epithelial cells, including the ability to form tight junctions and polarized monolayers, the Calu-3 model is a robust *in vitro* model for the respiratory endothelium. [61] A real-time monitored Calu-3 experiment indicated the uptake of fluorescent PS nanoparticles (50 nm diameter) after 3 hours of incubation. [30] While this demonstrated that Calu-3 cells can indeed internalize nanoplastics, it did not explore larger particles (0.1 – 1 μm).

The second cell culture model chosen was the U937 cell line, which was established from a human histiocytic lymphoma in the 1970s and has become a model for studying monocytes and macrophage differentiation. U937 cells are non-adherent, but can be differentiated into adherent macrophage-like cells by various stimuli, such as phorbol esters. [62] Modified PS nanoparticles (20–1000nm) were found to be internalized by differentiated U937 cells, with all particle sizes being internalized and demonstrating cytotoxicity. [63]

1.5. Gaps in Current Knowledge

As previously mentioned PS is the most commonly studied nanoplastic. [64] However, other widely used plastics, such as PP and PET, are underrepresented in nanoplastic research. These plastics differ in dispersity, density, and surface chemistry, leading to different interactions in biological and environmental systems. Consequently, more research is needed to investigate nanoplastics derived from PP and PET to better understand their toxicity, uptake, and behavior in biological systems.

One key challenge in nanoplastic research is the reporting of particle size. Studies commonly cite a single particle diameter, even though environmental nanoplastics are polydisperse and exist in a range of sizes. This polydispersity significantly affects particokinetics, including deposition, uptake, and cellular interactions. As such, reporting detailed size distributions rather than relying on single particle diameters is essential for producing more reliable and reproducible results. [65,66]

Current detection methods also present limitations. Microscopic techniques have a size detection threshold in the micrometer range, making it difficult to detect smaller nanoplastics. [67–69] Similarly, flow cytometry, while a key tool for quantifying cellular uptake, cannot typically detect particles below 300–500 nm, particularly in polydisperse samples, which stems from limitations in the optical resolution. [70] These detection challenges highlight the need for advanced methods that can reliably measure smaller nanoplastics and characterize polydisperse suspensions.

In summary, while PS dominates nanoplastic research, there is an opportunity to study PP and PET nanoplastics and improve both size reporting and detection methods. Addressing these gaps could lead to more accurate, reproducible, and biologically relevant findings.

1.6. Aims

This study was primarily motivated by the need for suitable nanoplastic reference materials to be used in *in vitro* and *in vivo* studies. Therefore, the first goal was to produce fluorescently labelled nanoplastic reference materials, specifically PET-F8BT and PP-F8BT, in the nano- size range. These materials were to address a critical need for standardized reference nanoplastics to enhance reproducibility in future studies.

In conjunction with the first goal, the next aim was to obtain nanoplastics with a low enough limit of detection and limit of quantification (LOD and LOQ, respectively) such that the nanoplastics could reliably be detected in *in vitro* experiments involving small amounts of material. Then the fluorescence reproducibility for these suspensions was to be determined by measuring calibration curves. Additionally, this thesis sought to characterize the size distribution of PET and PP nanoplastics in biorelevant media to evaluate the particle sizes to which cells were exposed in cell culture experiments.

Thereafter, the goal was to use computational models to predict the delivered dose based on size distribution as a benchmark for *in vitro* studies and uncover differences between PET and PP particles. Finally, a mass-based fluorescence uptake assay in a respiratory cell culture model to investigate the potential for PET and PP nanoplastics to cross the lung epithelium was to be performed. The outcome of the experiments listed above were chosen.

2. Materials

The following materials were utilized for the experiments:

0.22 µm membrane filters (Sigma-Aldrich, GSWP04700) and 0.8 µm nylon membrane filters (Whatman, 7408-004) for filtration; 24-well plates (VWR, 734-2325) for uptake experiments; 96-well plates (VWR, 734-2327) for MTT assays and calibration curves.

Calu-3 cells (ATCC HTB-55, LGC Standards) were used for cellular uptake and MTT experiments; DMEM/F12 medium (Thermo-Gibco, 31331093) was used to culture Calu-3 cells; PEG-400 (Sigma-Aldrich, CAS 25322-68-3) was used in MTT assays. Fetal bovine serum (FBS Superior, Merck Biochrom, S0615) and penicillin/streptomycin (10000U/ml, Thermo Fisher-Gibco, 15140122) were used to supplement the cell culture medium.

DMSO (≥99.5%, Avantor, A3672.0050) was used as a solvent; Triton X-100 (Sigma-Aldrich, T8787) was used for cell lysis; trypan blue (0.4%, Thermo-Fisher, 15250061) for cell counting; trypsin-EDTA (0.25%, Thermo-Fisher, 25200056) to detach adherent cells; phorbol 12-myristate 13-acetate (PMA, Sigma-Aldrich, 524400) was used for U-937 cell differentiation; U-937 cells (ATCC CRL-1593.2) were used for calibration curves; RPMI-1640 medium (Sigma-Aldrich, R8758) was used to culture U-937 cells.

F8BT (Mn ≤ 25,000, Sigma-Aldrich, CAS 210347-52-7) was obtained for fluorescence labeling; glycerol (Sigma-Aldrich, 8.18701.100) was used to suspend MNPs; polyethylene terephthalate (PET) granular (Goodfellow, ES30-GL-000112) and polypropylene (PP) granular (Sigma-Aldrich, CAS 9003-07-0) were used as starting materials for MNP production; Tween® 80 (Sigma-Aldrich, 9005-65-6) was used in particle suspensions for size measurments; xylene (Sigma-Aldrich,CAS 71-43-2), benzyl alcohol (99%, Sigma-Aldrich, CAS 100-51-6), and ethanol (96%, Brenntag, CAS 64-17-5) were used as solvents.

3. Methods

3.1. Production and Measurement of Suspensions

3.1.1. PET

PET was produced based on the nanoprecipitation method from Rosiuk, *et. al.* (2019) and NIPS protocols from Achilias, et. al. (2009) Lee, et.al. (2022) and Rodríguez Hernández (2019). First, 260 mg of PET pellets were added with 40 mL benzyl alcohol in a round bottom flask. The flask was heated in a silicon bath and stirred (250 RPM) under reflux at 220°C for 45 min until dissolved. The solution was then pipetted in a semicircular motion down the wall of a beaker containing 120 mL ethanol in an ice bath. The beaker was allowed to cool while stirring for 30 min.

F8BT-labelled PET (0.8% w/w, one batch and 5% w/w, one batch) were produced using a similar procedure to unlabeled PET, but under UV protection due to the light sensitivity of the dye. 260 mg PET pellets and 38 mL Benzyl alcohol were added to a round bottom flask with a magnetic stir bar and stirred (250 RPM) under reflux at 220°C in a silicon bath for 15 minutes. F8BT powder (0.8% w/w or 5% w/w) was dissolved in 2 mL benzyl alcohol and added to the refluxing flask. The setup was allowed to heat for another 30 minutes before precipitation.

3.1.2. PP

PP was produced according to an established and slightly adapted protocol. [43] First, ~350 mg PP pellets were added to a round bottom flask and stir bar with 40 mL xylene. The flask was heated in a silicon bath at 180°C under reflux stirring (250 RPM) for 30 min, after which the entire xylene solution was quickly transferred to a beaker with 160 mL stirring ethanol in an ice bath.

Fluorescent labelled PP-F8BT was produced with a 0.8% F8BT and 5% F8BT dye loading (one batch each) under light protection. PP pellets and xylene were added to a round bottom flask and stirred (250 RPM) at 180°C in a silicon bath under reflux for 15 minutes. F8BT powder (0.8% w/w or 5% w/w) was dissolved in 2 mL xylene and added to the round bottom flask. The solution was heated and stirred for another 15 minutes, followed by the precipitation step.

3.1.3. Filtration and Washing

Following precipitation in ethanol, all plastic suspensions were filtered and washed five times to remove residual solvents and replaced with ethanol. The suspensions were transferred to a Büchner funnel & flask vacuum filtration setup with a 0.8 µm membrane filter. Filtered ethanol (0.22 µm) was added in 100 mL increments (500 mL total) while stirring the mixture to break up larger plastic aggregations. The filter paper and filtrate were placed inside a pre-weighed flask which was filled with filtered ethanol (26 mL for PET and 35 mL for PP) and sonicated until agglomerates were dispersed, at which point the membrane filter was removed. The product was an approximately 10 mg/mL suspension of the plastic particles. Samples were sonicated for 90 minutes in a sonicator set to 35 KHz at 20°C.

3.1.4. Gravimetric Concentration Determination

To determine the exact concentration of the suspension, 1.0 g aliquot of plastic-ethanol suspension was added to a pre-weighed 2 ml vial and adhered to a rotary-evaporator (Rotary Evaporator VV 2011, Heidolph Instruments GmbH & co, Schwabach, Germany), then lowered into a water bath at 60°C. The pressure was decreased until the ethanol completely evaporated, indicated by a mass difference of less than 1% between consecutive measurements. The final mass was recorded, and concentration was determined by the following formula:

$$concentration\ \left[\frac{mg}{g}\right] = 1000 \cdot \left(\frac{m_{dry} - m_{empty}}{m_{wet} - m_{empty}}\right) \quad (4)$$

$$m_{empty} = mass\ of\ empty\ vial;\ m_{wet} = mass\ of\ vial + suspension;\ m_{dry} = mass\ of\ vial + plastic$$

3.1.5. Medium Change to Glycerol

The aim was to replace the suspension medium from ethanol to glycerol to make the suspension suitable for cell culture use. First, the plastic-ethanol suspension was transferred to a flask of known mass. Based on the gravimetric concentration determination, the mass of MNP powder was calculated. The mass of glycerol required to produce a 40mg/g suspension was added. The mixture was then warmed and sonicated until homogenous. The flask was carefully rotary-evaporated in a water bath (60°C) with

the pressure incrementally decreased. Ethanol was determined to be completely removed by repeatedly weighing the flask, with two consecutive readings of ≤1% mass difference. By subtracting the mass of glycerol and the empty flask, the final mass of plastic was determined, and yield and concentration were recorded.

$$m_p = m_{f\ wet} - \left(m_{f\ empty} + m_g\right) \quad (5)$$

$$m_p = mass\ of\ plastic;\ m_{f\ wet} = mass\ of\ flask + suspension;\ m_{f\ dry} = mass\ of\ empty\ flask;\ m_g = mass\ of\ glycerol\ added$$

3.1.6. Size Measurement via Static Light Scattering (SLS)

The size distribution of colloidal suspensions can be determined by measuring the intensity of light at different angles that have been scattered by small particles in suspension. This method, known as Static Light Scattering (SLS), can be used to measure particles similar to and larger than the wavelength of light by applying Mie theory. [71,72] While typically used to determine the molecular weight of proteins and polymers, the particle diameter can also be determined by assuming the particles are spherical and of homogenous density. The radius of gyration, R_g, is then used to determine to particle radius *r*. [73,74] SLS was chosen as it is effective for particle sizes that are larger than the wavelength of light and at least ≥ λ/20. [75] SLS quickly produces a size distribution curve in a non-destructive fashion, while also measuring the particles *in situ*, preserving the native characteristics of colloidal suspensions. [75]

Size measurements were recorded for all particle types when suspended in 10 mg/mL ethanol, and after the medium change to glycerol. Size measurements were performed using static light scattering (Mastersizer 3000, Malvern Panalytical, Malvern, United Kingdom). Particles were assumed to be spherical. For each batch of MNP suspension, measurements were recorded first in ethanol, then in glycerol. Samples were prepared by mixing plastic suspension with 5% w/w filtered (0.22 µm) Tween®80 (Tw80) (1:1). The Mastersizer cell was filled with 400 µL 5% Tw80 and then to the fill line with MilliQ H_2O. The sample was added in 10-20 µL increments and stirred at 700 rpm until an obscuration between 3–6% was achieved. Refractive indexes of the 1.33 (water and used for RPMI-1640), 1.63 (PET) and 1.49 (PP) were selected. Ten technical measurements were recorded, and the average was reported.

3.1.7. Dispersion protocol in Biorelevant Media

To attain a 1 mg/mL stock solutions of PET–F8BT and PP–F8BT (**first dilution**) the original 40 mg/g **glycerol stock** was heated for 10 minutes at 70ºC and vortexed for 30 sec. A 30 second vortex and 2-minute heating step was then repeated for a total of three times. Finally, the sample was sonicated at 35 KHz for 3 minutes. 3-6 drops of the glycerol stock were weighed. Diluting the original **glycerol stock** (40 mg/g) with 20% of a 5x concentrated solution of FBS in H_2O (50%) produced a final 10% FBS concentration in the **first dilution**. The formulas for determining the volume are:

$$5x\ FBS = mass_{FBS} + V_{H2O} \quad where \quad V_{H2O}\ [\mu L] = (2 * 1000 * mass_{FBS}) \tag{6}$$

$$V_{5x\frac{FBS}{H2O}}[\mu L] = \frac{m_{MNP\ suspension}\ [g] \cdot 40\ \left[\frac{mg}{g}\right] \cdot 1000\ [\frac{\mu L}{mL}]}{1\ [\frac{mg}{mL}]} \tag{7}$$

$$V_{5x\ FBS} = 0.2 \cdot V_{5x\frac{FBS}{H2O}} \tag{8}$$

$$V_{H2O} = V_{5x\frac{FBS}{H2O}} - V_{5x\ FBS} \tag{9}$$

The **first dilution** was further diluted with sterilized H_2O and DMEM/10% FBS to 100 µg/mL and 50 µg/mL (**second dilution)**. FBS/sterilized H_2O was required to prevent the loss of water from the cells due to osmotic pressure from glycerol. Water and the suspensions were vortexed until well mixed. Volumes were calculated as follows:

$$V_{H2O}\ [\mu L] = 4 \cdot V_{MNP\ sus.} \tag{10}$$

$$V_{DMEM} = V_{total} - (V_{MNP\ sus.} + V_{H2O}) \tag{11}$$

The measurement cell was filled with H_2O+5x FBS or RPMI-1640, the background was recorded, and MNP suspension in H_2O+5x FBS or RPMI-1640 was added in 10-20 µL increments.

3.2. Calibration Curve Protocol

3.2.1. U937 Cell Culture and Differentiation Protocol

U937 cells (ATCC: CRL-1593.2) were cultured in completed RPMI-1640 (10% FBS + 1% penicillin/streptomycin) medium. They were seeded in 24 well plates with a cell density of 2 x 10^5 cells/mL by adding 500 µL of cell suspension to wells which already contained 500 µL of 200 nM Phorbol-12-myristate-13-acetate (PMA) in RPMI-1640 (final concentration 100 nM PMA). Cells were differentiated for 48h at 37°C, 5% CO_2.

3.2.2. Sample Preparation

The **first dilution** (1 mg/mL) of each MNP type were produced by following the dispersion protocol described in chapter **3.1.7**. A serial dilution was setup for seventeen concentrations (500 µg/mL to 0.008 µg/mL) with PBS and U937 lysate as dispersants. Samples were prepared in n=3 technical replicates and n=3 biological replicates.

3.2.3. Fluorescence Measurement

100 µL of each sample were pipetted into 96 well plates and the fluorescence was recorded on a plate reader (Tecan infinite 200Pro, Tecan i-control software). Plates were measured without a lid, with orbital shaking (60 seconds, 1 mm amplitude) at 460 nm excitation and 521 nm emission wavelengths. Analysis was performed in excel and statistical analysis by regression. LOD and LOQ were determined by the following formulas [76]:

$$LOD = \frac{3.3 \cdot \left(SE_{intercept} \cdot \sqrt{n}\right)}{m_{x\ variable}} \tag{12}$$

$$LOQ = \frac{10 \cdot \left(SE_{intercept} \cdot \sqrt{n}\right)}{m_{x\ variable}} \tag{13}$$

Where n is the number of points analyzed, and $SE_{intercept}$ and $m_{x\ variable}$ are the standard error of the y-intercept and coefficient of the x variable, respectively.

3.3. Uptake Dosimetry Modelling

3.3.1. ISDD

The ISDD program, downloaded free of charge from pnnl.org, was executed through MatLab®, version R2020b. Constants used for calculations were as follows: density of PET: 1.38 g/cm^3; density of PP: 0.9 g/cm^3. Initial particle concentrations were 250 and 500 µg/mL (PET), and 1000 and 2000 µg/mL (PP). Additional parameters were: volume of cell culture medium inside the plate (0.5 mL); height of liquid column in each well = 2.85 mm; temperature (37 °C); medium density (1.002 g/cm^3); medium viscosity (0.738×10^{-3} Pa·s) [32]; Particles were assumed not to aggregate. Simulations were run for 24 hours with 97 data points printed and grid size of 1501. Mean particle diameter was used for each size class, e.g. for 100-200 nm size class, particle diameter of 150 nm was input into ISDD. “Fraction Deposited” was printed and used for data analysis in Microsoft Excel® for Mac.

3.3.2. RiskGone *In Vitro* Dosimetry

The input parameters included the particle size distribution (measured via SLS), particle density (PET = 1.38 g/cm^3 and PP = 0.90 g/cm³), particle concentration (PET = 250 and 500 µg/mL; PP = 1000 and 2000 µg/mL), medium density (1.002 g/mL), medium viscosity (0.738 mPa·s), medium height (2.85 mm), well bottom surface area (1.9 cm^2), temperature (37 ºC), and exposure duration (24 hours). “Sticking bottom” was not selected. Additional parameters were: height of subcompartment (0.005 mm), centrifugation (1), time interval for simulation (0.5 s). “Bottom area only” was selected and results were printed for 30-minute intervals.

These parameters were entered into the freely provided RiskGone *In Vitro* Dosimetry application. (https://www.enaloscloud.novamechanics.com/riskgone/InVitroDosimetry). [77] Fraction Deposited was printed and used for data analysis in Microsoft Excel® for Mac.

3.4. Calu-3 Uptake

3.4.1. Cell Seeding

Calu-3 cells (Lung adenocarcinoma; Human; ATCC-HTB-55) were used to investigate nanoparticle uptake. Cells were seeded at a density of 2×10^5 cells/mL in a 24-well plate and cultured in completed DMEM (10% FBS + 1% penicillin/streptomycin). The cells were incubated at 37°C with 5% CO_2 for 24 hours to allow for adhesion and growth. A control blank plate was prepared under the same conditions, but no cells were added.

3.4.2. PET–F8BT (5%) and PP-F8BT (5%) Dispersion Protocol

To prepare the samples, the dispersion protocol from **3.1.7** was used. Samples were prepared into a 10 mg/mL stock, then diluted to 500 μg/mL and 1000 μg/mL for PET–F8BT (5%), and 2000 μg/mL and 4000 μg/mL for PP–F8BT (5%).

3.4.3. Uptake Protocol

Post-seeding time and washing, 250 μL of medium and 250 μL of MNP suspension (final concentration: 250 μg/mL and 500 μg/mL PET–F8BT (5%); 1000 μg/mL and 2000 μg/mL PP–F8BT (5%) were added to the plates and then incubated at 37°C with 5% CO_2 for 3 hours. The medium including the treatment was aspirated, and the cells were washed three times with 1 mL PBS to remove non-internalized nanoparticles. The monolayer was then air-dried, protected from light, at room temperature for 18 hours. The dried cell monolayer was resuspended in 1 mL Triton-X in PBS (0.1%). Fluorescence measurements were recorded on a Tecan infinite 200 pro using Tecan i-control software. The excitation wavelength was 342 nm and emission wavelength 542 nm. The initial pilot experiment was performed using n=1 passage number (P25), and the second experiment was performed with P22.

3.5. PEG-400 MTT Assay

3.5.1. Calu-3 Cell Culture

Calu-3 cells (passage numbers: P24, P26, P31) were seeded in completed DMEM (10% FBS + 1% penicillin/streptomycin) at a density of 4 x 10^5 cells/ml in 96 well plates, then incubated at 37°C with 5% CO_2 for 24 hours.

3.5.2. Sample Preparation

PEG-400 in completed DMEM (50% w/v) was further diluted to the following final PEG-400 concentrations: 400, 200, 100, 50, 25, 12.5, 6.25, 3.13, 1.56, 0.78 µg/mL. . Triton X (0.25%) was prepared as the negative control and untreated wells as the positive control.

3.5.3. MTT Assay

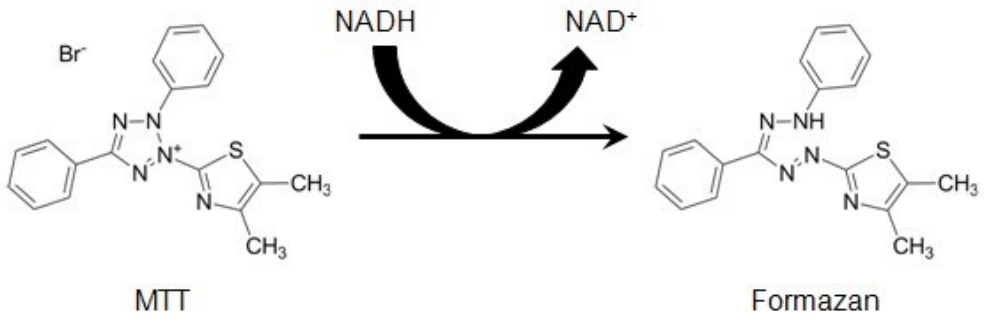

Figure 3. Structures of MTT and colored formazan product. (Riss, *et. al.* 2013) [78]

The MTT assay is a colorimetric method used to assess cell viability by measuring metabolic activity. The principle of the assay is based on the ability of viable cells to reduce the yellow tetrazolium salt MTT (3-(4,5-dimethylthiazol-2-yl)-2,5-diphenyltetrazolium bromide) into purple formazan crystals (**Figure 3).** [79] This reduction occurs in the mitochondria of metabolically active cells through the action of NAD(P)H-dependent oxidoreductases. The amount of formazan produced is proportional to the number of living cells and can be quantified by dissolving the crystals in DMSO and measuring the absorbance at 570 nm using a spectrophotometer. [80]

MTT was conducted to assess the cytotoxicity of PEG-400 on Calu-3 cells. [81] The medium was removed from the 96-well plates and 100 µL completed DMEM was added to each well. Subsequently, 100 µL of each respective PEG-400 dilution was added. The cells were then incubated at 37°C with 5% CO_2 for 24 hours. 20 µL of syringe filtered-sterilized (0.22 µm) MTT in PBS (5 mg/mL) was added to each well. After 3.5 hours, the liquid was drained and 100 µL of DMSO was added and mixed for 15 minutes. The plates were read in a UV plate reader (BioTek® Epoch 2 Microplate Reader) with orbital shaking (1 min, 425 cpm, 3mm). The absorbance at 570 nm was recorded. Viability was determined using the measured absorbances with the equation:

$$Cell\ Viability\ (\%) = 100 * \frac{T - N}{P - N} \tag{14}$$

$T = test\ well\ absorbance; N = negative\ control\ (TritonX\ 0.25\%)\ absorbance;$
$P = positive\ control\ (untreated\ cells)\ absorbance$

Analysis was performed in Microsoft Excel® by fitting a three parameter logistic equation to the viability data.

3.6. Statistics

Statistical analysis was performed with Microsoft Excel® for Mac, version 16.66.1. Statistical significance was determined by ANOVA single factor analysis with $\alpha = 0.05$. P-value ≤ 0.05 indicated that the data was significantly different. Denotation: * $p < 0.05$, ** $p < 0.01$.

4. Results and Discussion

4.1. Is it possible to produce nano-sized PET–F8BT and PP–F8BT suspensions?

To increase cohesion between studies investigating nanoplastics, the need for a suitable reference material has been identified as a major focal point. Thus, this work attempted to produce nanoparticles in the 0.1 – 1.0 µm size range. PET and PP were chosen specifically due to the lack of available reference materials for these plastic types, as well as broadening the types of plastics studied given the different physical and chemical characteristics between PET and PP. PP is lower density (~0.9 g/cm^3) than aqueous medium used in cell culture, while PET is denser (1.38 g/cm^3), which could lead to vastly different behavior in biological systems. PP is also more hydrophobic than PET,

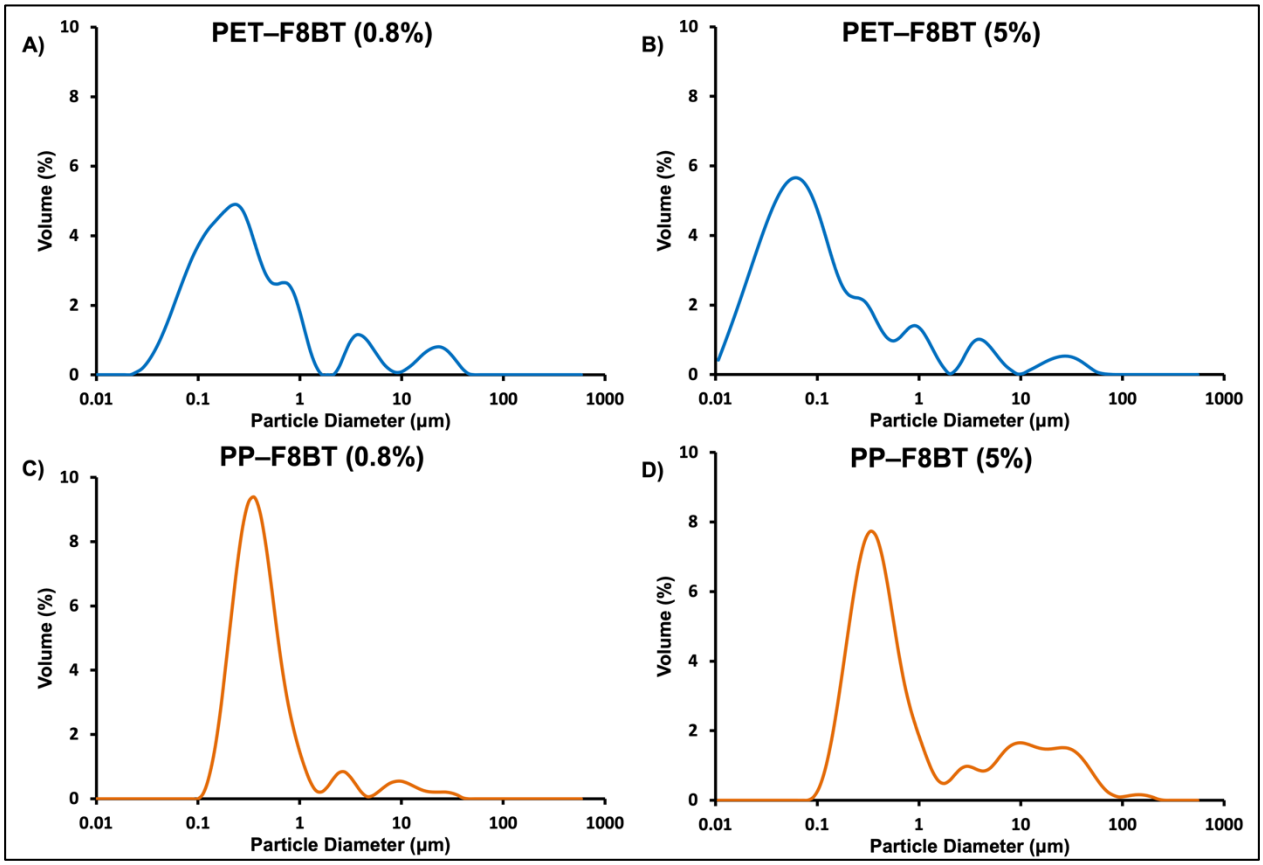

Figure 4. SLS size distributions in glycerol of F8BT-labelled MNP suspensions produced by NIPS method for **A)** PET–F8BT (0.8%), n=1 batch; **B)** PET–F8BT (5%), n=1 batch; **C)** PP–F8BT (0.8%), n=1 batch and **D)** PP–F8BT (5%), n=1 batch.

and since the particles were suspended in aqueous media, aggregation was hypothesized to lead to larger PP size distributions.

In this section, one batch each of PET–F8BT (0.8%), PET–F8BT (5%), PP–F8BT (0.8%) and PP–F8BT (5%) were produced, and the size distributions measured in glycerol are reported. The size distribution of PET–F8BT (0.8%) in **Figure 4A** shows a major peak between 0.05–1.1 μm, with two minor peaks extending to over 100 μm. The values Dx(10) = 0.09 μm and Dx(50) = 0.25 μm indicate a vast majority of the suspension was below 1 μm, while large particles are still present based on the Dx(90) = 14.75 μm. The size distribution of PET–F8BT (5%) (**Figure 4B**) reveals a significant portion of particles below 0.1 μm, with three minor peaks extending up to 50 μm. The Dx(10) and Dx(50) values were measured at 0.02 μm and 0.08 μm, respectively. Additionally, the Dx(90) value of 1.31 μm indicated the presence of large particles in the upper boundary, which accounted for a small but significant portion of the suspension.

PP–F8BT (0.8%), shown in **Figure 4C**, has a much tighter peak between 0.1–1.0 μm and overall a much tighter distribution. The Dx(10) = 0.077 μm, Dx(50) = 0.265, and Dx(90) = 3.87 μm values demonstrate the lower degree of polydispersity in comparison to PET. **Figure 4D** depicts PP–F8BT (5%), with a single major peak between 0.1 – 1.0 μm, along with a broad, flat peak extending to 100 μm. The Dx(10), Dx(50), and Dx(90) values for PP of 0.20 μm, 0.49 μm, and 20.42 μm, respectively, indicate similar results to the 0.8% batch but with more large particles.

Sub-micron, nile-red labelled PET nanoplastics have been produced by reprecipitation in trifluoroacetic acid. [48] However, the current work appears to be the first to produce F8BT-labelled nanoplastics with benzyl alcohol as the solvent. Likewise, nile-red labelled PP has been produced [43] and the Dx(50) values from this experiment (0.265 μm, 0.8%; 0.49 μm, 5%) are consistent with the average diameter of 0.562 μm reported by Lee, *et. al.* (2022). The PET–F8BT and PP–F8BT nanoparticles should be further investigated to confirm if the chemical composition of the polymers is preserved, which could be achieved by FTIR. [43]

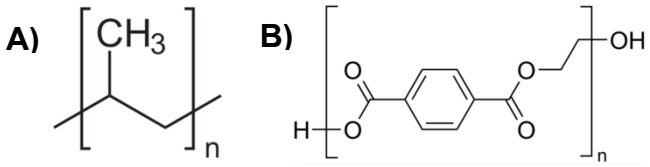

Figure 5. Monomeric unit of **A)** polypropylene and **B)** polyethylene terephthalate.

Additionally, these results could be improved by eliminating the large particles present in the SLS data. These are likely aggregates formed due to the hydrophobic nature of both plastics in glycerol. **Figure 5A** highlights the highly hydrophobic nature of PP, consisting only of a methylated carbon backbone. Meanwhile, PET (**Figure 5B)** could accept hydrogen bonds in an aqueous solvent, but it is still categorized as hydrophobic. [82] The small particles have a very high surface area and are concentrated to 40 mg/g in hydrophilic glycerol, and although it has been shown to stabilize proteins in solution [83], glycerol does not appear to stabilize PP or PET enough to eradicate aggregation. Previously, large aggregates have been removed by allowing the suspension to settle, then measuring only the supernatant containing the colloidal particles. [43,48,84,85] This method significantly decreases yield, which is a major downside for preparing particles at a reference material scale. Another solution would be to decrease the concentration of plastics, decreasing the likelihood of particles coming into contact with each other, as this principle has been demonstrated with PS in water, albeit at much lower concentrations. [86]

The volume of particles below 0.1 μm is unique to PET, especially PET–F8BT (5%). This is approaching the lower measurement limit of $\lambda/20$. [75] This effect is not present in PP and amplifies from 0.8% F8BT to 5% F8BT, which might indicate F8BT nanoparticles forming independently from the PET particles since they are only present with the higher dye loading percentage. Chemical identification methods, such as FTIR [14], would be necessary to confirm the composition of these particles.

In summary, PET and PP with both 0.8% and 5% F8BT loading can be produced in the 0.1 – 1 μm range, but large aggregates are present in every sample type. Further method refinements, such as sonication time and centrifugation followed by the separation of the supernatant may be necessary to remove these large particles.

4.2. What are the fluorescence characteristics of PET–F8BT (0.8%) and PP–F8BT (0.8%)?

The goal of the producing calibration curves with the MNP suspensions was to determine the LOD and LOQ values and examine the reproducibility between technical replicates and biological replicates (batch-to-batch variation), in addition to any effects cell lysate compared to PBS as a dispersant might have on the fluorescence. It was hypothesized that PP would have a higher LOD than PET due to the tendency for PP to float and aggregate, which would possibly decrease fluorescence intensity by decreasing the total particle surface area, quenching fluorescence. Additionally, it was thought that U937 lysate would coat the nanoparticles with biological components, but it was unclear whether that would have a fluorescence quenching effect or increase the fluorescence.

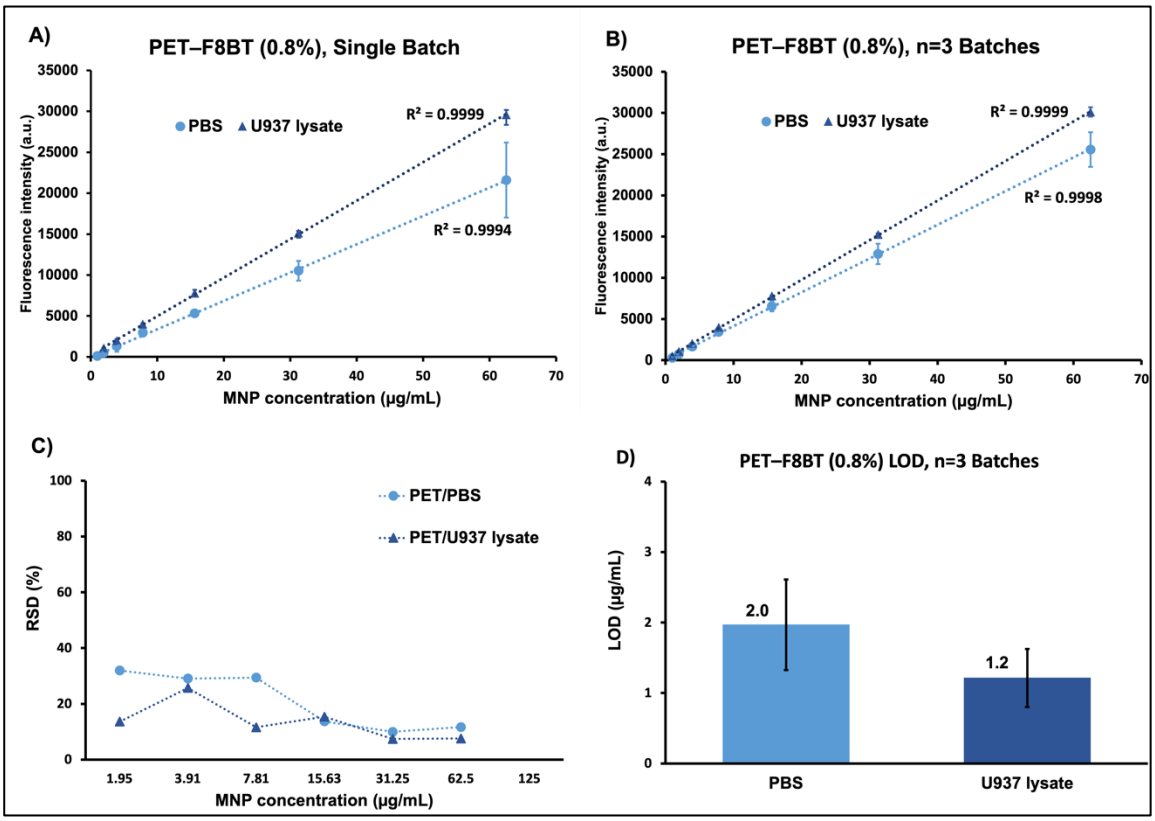

Figure 6. Calibration curves are plotted for **A)** PET–0.8% F8BT, (n=3 technical replicates) and **B)** PET–0.8% F8BT **(**n=3 batches) dispersed in PBS and U937 lysate. **C)** RSD (%, n=3 batches) plotted for PET–F8BT (0.8%). **D)** LOD values (n=3 batches) are plotted in both PBS and U937 lysate.

Figure 6A and **6B** depict the PET–F8BT (0.8%) calibration curves for n=3 technical replicates and n=3 batches, respectively. The relative standard deviation (RSD) values (**Figure 6C**) remained between 5-40% in both PBS and U937 lysate, with U937 lysate

having slightly lower RSDs for all concentrations. **Figure 6D** depicts the mean LOD (n=3 batches) in both dispersants, with PBS = 2.0 ± 0.6 µg/mL and U937 lysate = 1.2 ± 0.4 µg/mL.

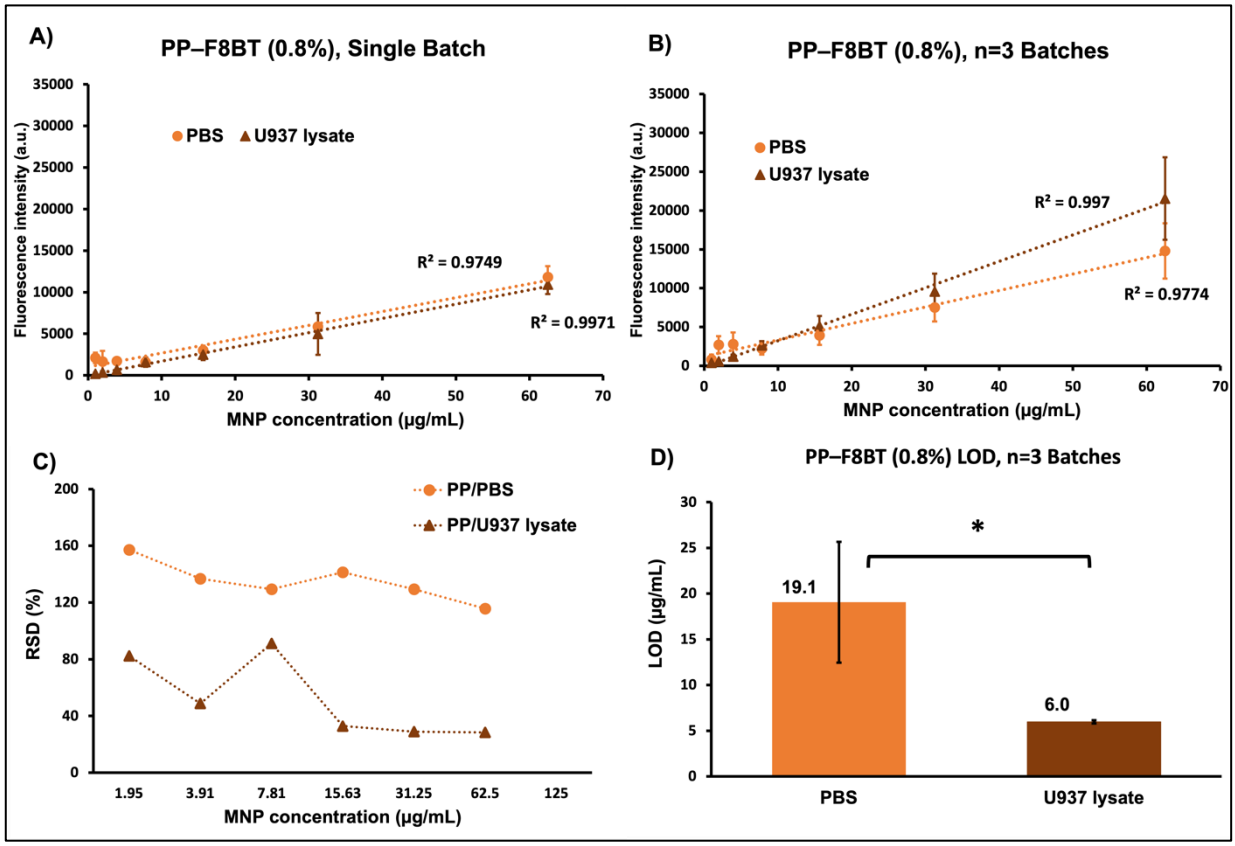

Figure 7. Calibration curves are plotted for **A)** PP–0.8% F8BT, (n=3 technical replicates) and **B)** PP–0.8% F8BT (n=3 batches) dispersed in PBS and U937 lysate. **C)** RSD (%, n=3 batches) plotted for PP–F8BT (0.8%). **D)** LOD values (n=3 batches) are plotted in both PBS and U937 lysate.

PP–F8BT (0.8%) is shown in **Figure 7A** and **7B**, with calibration curves for n=3 technical replicates and n=3 batches, respectively. The RSD values (**Figure 7C**) are higher than in PET, ranging from 30-160%, with PBS values approximately double the U937 values. **Figure 7D** depicts the mean LOD (n=3 batches) in both dispersants, with PBS = 19.1 ± 6.6 µg/mL and U937 lysate = 6.0 ± 0.2 µg/mL.

PP had a significantly lower LOD value in U937 lysate than in PBS. This difference could have originated from a difference in aggregation between dispersants, which lowers the surface area per mass ratio and in turn decreases the fluorescence detected. The proteins and lipids present in the U937 lysate but absent in PBS might stabilize individual PP particles by acting as adhering to the particle surface and acting as surfactants, with this effect being more prominent for PP because the larger aggregates would be more

buoyant. The protein corona formation has been well described in several nanoparticle studies. [31–33]

The data in **Figure 6** and **Figure 7** present PET to be much more reproducible than PP. This at first seems surprising because PP (**Figure 4C, 4D**) is much less polydisperse. Instead, the driving force behind the difference in LOD stems from the different physical and chemical characteristics of the plastics. PP has a density of ~0.9 g/cm^3 whereas PET is denser (1.38 g/cm^3). This, in addition to the difference in hydrophobicity and evidence that PP aggregates more readily, could lead to the lack of reproducible fluorescence readings for PP. In the well plate, PP floats to the surface of the medium, aggregates and collects on the edge of the well along the meniscus. PET remains in suspension, sinking to the bottom over time. Since the plate reader did not measure at the edge of the well, a non-representative fluorescence reading explains the higher-than-expected LOD value. Additionally, this supports the observation that RSD values are significantly higher in PBS. While the protein corona inhibits the aggregation effect in U937 lysate, PBS measurements are subject to more random chance fluorescence variations because aggregated MNPs are less homogenously dispersed leading to less consistent fluorescence measurements.

The structure of the nanoparticles also needs to be investigated. The oxidation state of the components, as well as the distribution of F8BT among the PET and PP could affect the fluorescence. F8BT has varying quantum efficiencies in different oligomeric states [52] and if there is a different substructure between the PET nanoparticles and PP nanoparticles, there could be variations in the fluorescence.

Likewise, labelling efficiency between polymer types could also explain some variation. Since the detection method is mass-based, if there are significant differences in the amount of F8BT retained in the plastics, then the LOD would change. Further, since the plastics are co-polymerized with F8BT, if the dispersion is very heterogenous, a similar effect would be observed. Standardization of the MNP production protocol should involve FTIR and fluorescence measurements of the particles to confirm consistency and longevity of their fluorescence. [87]

The LOD for PET shows promise for use in uptake experiments, as it is low enough to be quantifiable, when using other nanoparticle uptake experiments in Calu-3 and macrophages as a benchmark.[30,32]

4.3. Is the dispersion protocol effective?

To determine the effect of cell culture medium on particle diameter, as well as investigate the efficacy of the dispersion protocol in suspensions were prepared as per **3.1.7,** except using PET–F8BT (0.8%) and PP–F8BT (0.8%) dispersed in RPMI for the 100 µg/mL. It was hypothesized that aggregation would increase after being introduced to the aqueous medium, but that FBS could act as a dispersant like Tw80 and preserve the colloidal behavior. The 5x concentrated FBS was used to prepare the dilutions with the goal of dispersing the suspensions.

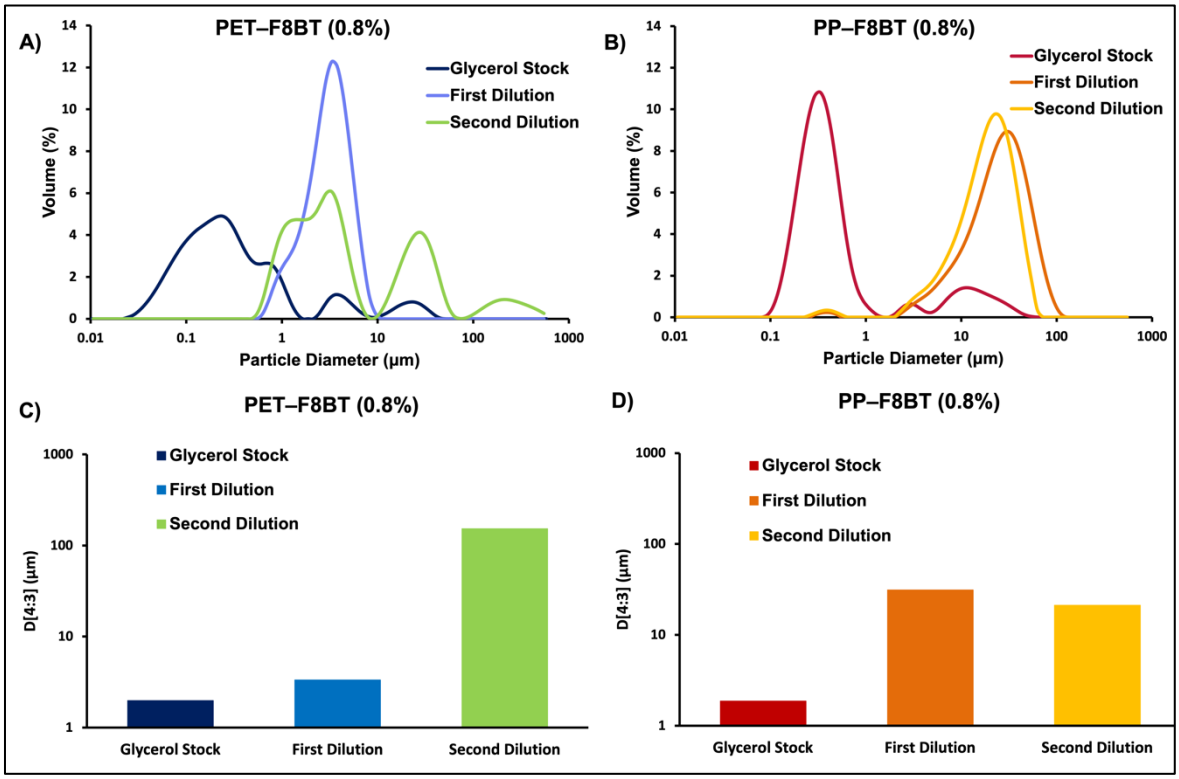

Figure 8. SLS measurement of **A)** PET–0.8% F8BT and **B)** PP–0.8% F8BT, in three suspensions: glycerol stock, first dilution (1mg/mL MNP in H20+FBS) and second dilution (100 µg/mL MNP in RPMI). Volume-weighted mean diameter, D[4;3], of **C)** PET (n=1 batch) and **D)** PP (n=1 batch).

The PET dispersions in **Figure 8A** show that particle size drastically increases in the first dilution, with almost no volume below 1 µm and aggregates over 100 µm in diameter. Visual inspection confirmed this, as aggregates were visible to the naked eye, even after 10- and 25-minute sonication intervals. The portion over 100 µm could also be bubbles, which form upon mixing with the FBS. Interestingly, when the particles were suspended in RPMI, polydispersity decreased and there was only one major peak between 0.8–10µm. This effect was surprising, considering the relative concentration of FBS was higher in the first dilution. These observations were also present in the PP measurements

(**Figure 8B)**, although the degree of polydispersity was much lower, with the maximum size being limited to around 100 µm. **Figure 8C** and **8D** are plots of the De Brouckere mean diameter, D[4;3], which is a sensitive parameter towards large particles based on volume. [88] Both PET and PP display significant increases in D[4:3] with the first and second dilution, indicating the dominance of large particles in the overall particle volume.

The increase in aggregation between the glycerol stock and first dilution is not surprising, because the difference is viscosity between glycerol (1455 mPa·s, 293 K) [89] and water (1 mPa·s, 293 K) [90] is stark, and subsequently chance that small particles will interact and agglomerate in the prescence of water is greatly increased. [91] The less drastic change in particle diameter between the first dilution and second dilution suspensions compared to the glycerol stock may stem from the buffering capacity, which is much higher in RPMI due to the presence of salt buffers. It is not clear how the presence of buffers would affect the stability of a suspension of particles with adsorbed proteins on their surface, but assuming that the particles are coated in proteins in both water and RPMI, the buffers could reasonably stabilize the protein-protein interactions, leading to less aggregation. [92–94] Further characterization of the protein coronas on PET and PP nanoparticles would be necessary to elucidate this process.

4.4. Do ISDD and *In Vitro* Dosimetry predictions indicate significant particle deposition?

To estimate the cellular dose of nanoparticles in the *in vitro* uptake study, the RiskGone *In Vitro* Dosimetry web application and ISDD were employed. A simulated uptake experiment was performed, using the parameters from the *in vitro* experiment to estimate the delivered dose. The predicted delivered dose values were hypothesized to be larger than the experimental ones, because the computer models do not measure internalization of nanoparticles, but rather all particles which reach the bottom of the well

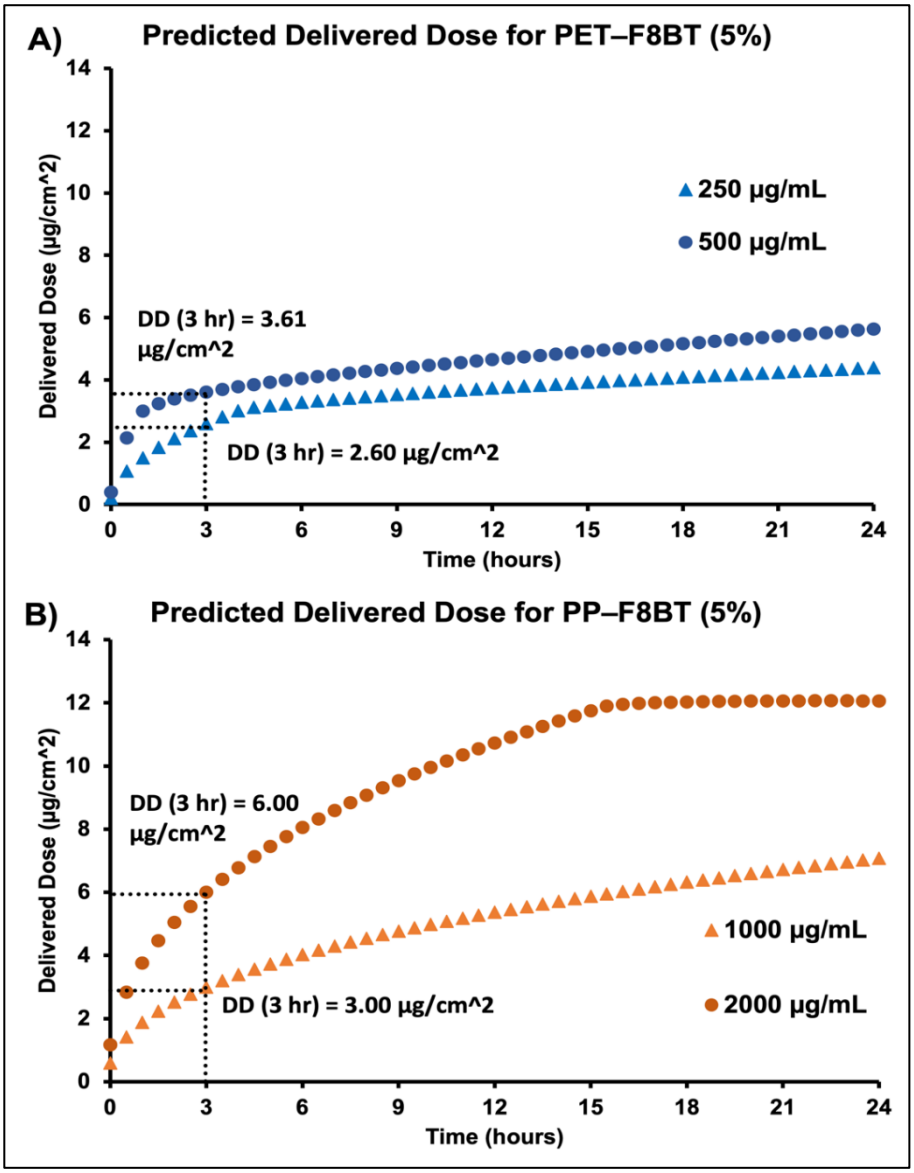

Figure 9.Computationally predicted delivered dose (DD) values from RiskGone *in vitro* Dosimetry.

plate. PET was therefore predicted to have higher delivered dose values than PP due to the difference in density.

Table 1 shows the delivered dose values calculated using ISDD and RiskGone *in vitro* Dosimetry, and the first observation is that ISDD results are much higher than RiskGone, which stems from the "sticky" boundary condition in ISDD, meaning that every particle which reaches the bottom of the well counts as deposited. Meanwhile "non sticking" boundary was chosen for RiskGone. [77] Additionally, RiskGone natively performed calculations with the particle size distributions, while ISDD required scaling a series of single diameter predictions with the size distribution data. Both programs were given distributions of 0.1 – 1.0 µm in size and assumed no particle aggregation.

Table 1. Delivered dose values calculated from ISDD and RiskGone *in vitro* Dosimetry.

	PET–F8BT (5%)		**PP–F8BT (5%)**	
	250 µg/mL AD	500 µg/ml AD	1000 µg/mL AD	2000 µg/mL AD
RiskGone *in vitro* Dosimetry DD (µg/cm^2)	2.60	3.61	3.00	6.00
ISDD DD (µg/cm^2)	13.80	27.59	27.46	45.48

A surprising result in **Figure 9A, 9B** is the apparent deposition of PP. This was contrary to the hypothesis that very little PP would deposit due to its higher buoyancy, but in fact particles deposit steadily until they begin to stagnate. This effect might arise from the colloidal behavior of small particles, which move throughout the suspension driven by collisions with other small particles and dispersant molecules. [75,91] Larger PP particles would be driven to the well surface by buoyancy, but the colloidal sized particles have a significant change of depositing on the well bottom due to Brownian motion. [35]

Another valuable piece of information from this graph is the deposition rate, which greatly slows down after t = 3-hours. This suggests a 3-hour timepoint for the *in vitro* experiment is suitable point to measure uptake.

4.5. Is there measurable MNP uptake in Calu-3 cells?

The goal of the uptake experiment was to first determine if there was measurable fluorescence with two administered doses (AD) of PET–F8BT (5%) and PP–F8BT (5%). It was hypothesized that PET would deposit onto the cell membrane and produce a signal because PET has a higher density than the cell culture medium and the particles would sediment. PP was predicted to have a much lower signal, since it is buoyant in cell culture medium. Additionally, the aim was to determine how significant background noise would be an issue since any sticking of the MNPs to the well plate would interfere with the fluorescence reading. The washing protocol was thought to mitigate this issue, but for each experiment a blank plate (without cells, with MNP) treated under identical conditions was prepared.

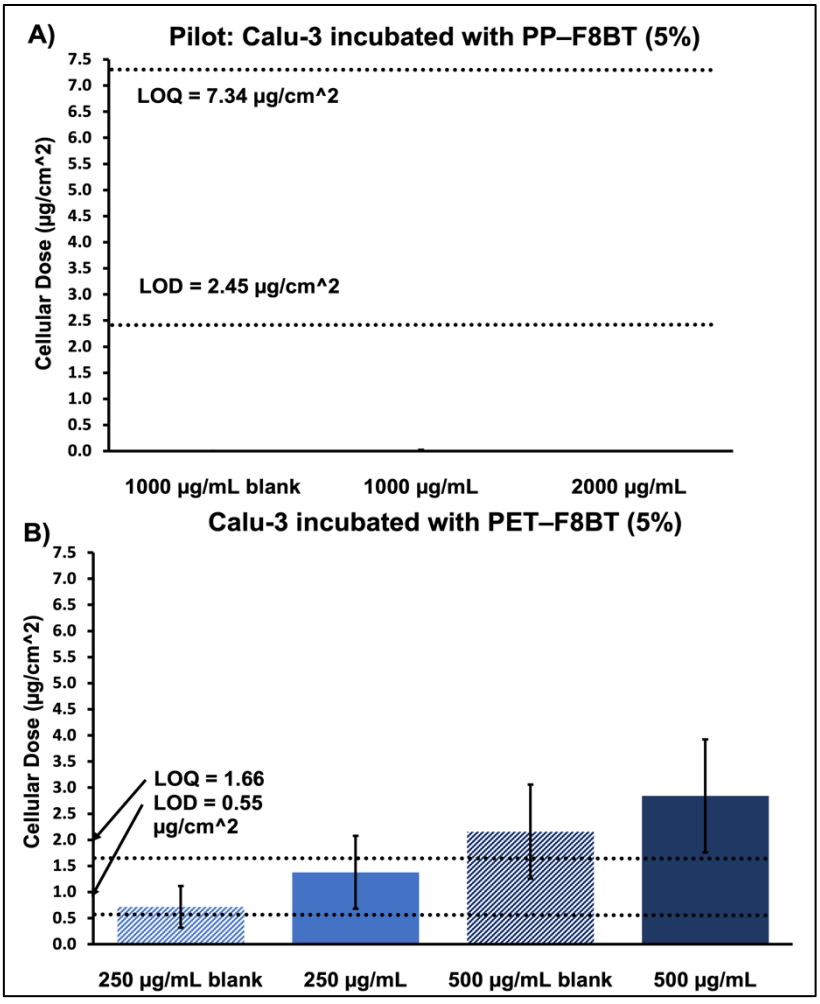

Figure 10. A) The pilot uptake experiment performed in Calu-3 with PP–F8BT (5%). B) uptake take experiment performed with Calu-3 and PET–F8BT (5%) with n=1 passage numbers. Note: LOD/LOQ data was obtained from a calibration curve done by another operator.

Prior to this uptake experiment, another operator determined the LOD/LOQ of PET–F8BT (5%) and PP–F8BT (5%) for the batches used in this experiment. These values are are plotted as horizontal lines on the graphs in **Figure 10**.

A pilot uptake experiment was performed with both PET (not shown) and PP (**Figure 10A)**, and the results indicated PET–F8BT (5%) had measurable uptake but PP–F8BT (5%) displayed virtually no measurable uptake. Therefore, the decision was made to perform the full experiment only with PET. **Figure 10B** depicts the results, with the uptake values above the LOD for all conditions, and above the LOQ for the 500 µg/mL AD condition. The uptake values in **Table 2** show the significant amount of MNP that remained on the blank plate in comparison to the test plate. This result indicates that particles sticking to the edge or bottom of the well, independent of cells, create uncertainty in the uptake values.

Table 2. Uptake of PET–F8BT (5%) with Calu-3.

Calu-3 incubated with PET–F8BT (5%) for 3 hours		
	Cellular Dose (µg/cm^2)	SD±
250 µg/mL blank	0.72	0.4
250 µg/mL	1.38	0.7
500 µg/mL blank	2.16	0.9
500 µg/mL	2.84	1.1

These results imply that some particles were internalized into the cells and stuck on the cell surface, while others were stuck to the plate. There are several possibilities for addressing this source of error, with lower concentrations of administered doses and an improved washing protocol offering some potential decrease in the sticking particles.

To make this method more robust, the dispersion protocol must be improved such that large aggregates are not present in the suspension, and only colloidal sized particles are being exposed to the cells. It could be achieved by using a lower concentration MNP stock that has been freshly prepared. The limitation is the concentration of glycerol, which is hyperosmotic. With lower MNP stock concentrations, the relative amount of glycerol would increase, and it is crucial to avoid high concentrations of glycerol in the cell suspension to prevent cytotoxic effects. MTT results produced in the Dailey

laboratory indicated that concentrations of glycerol over 2.5% *w/v* induced cytotoxic effects. The glycerol concentrations in this experiment were equivalent to 0.625% – 5% *w/v*, which likely had no visible effect on the uptake results, as the glycerol concentration for the PET data was 0.625% *w/v* (250 µg/mL AD) and 1.25% *w/v* (500 µg/mL AD). For PP, it had no effect as there was no detectable uptake.

PP, on the other hand, would require a different experimental setup to determine uptake. One possible solution is an inverted cell culture setup, which places the cell monolayer at the top of the well, providing buoyant particles exposure to the cell membranes. Inverted well plates have already been used to investigate PP and PE cytotoxicity and are a promising option to further investigate buoyant nanoplastics. [95,96]

4.6. Is PEG-400 a suitable MNP suspension medium?

The MTT assay was performed with PEG-400 on Calu-3 cells to determine the cytotoxicity to evaluate its suitability as a nanoplastic suspension medium to replace glycerol. The main reason an alternative to glycerol was sought was to find a medium with a lower cytotoxicity. Glycerol concentrations above ~2.5% *w/v* were identified to decrease cell viability below 70%, and yet higher concentrations may be necessary to deliver higher concentrations of MNP to the cells. PEG-400 has been shown to have a slightly lower cytotoxicity than glycerol in similar experiments. [97] Therefore it was hypothesized that PEG-400 would exhibit lower cytotoxicity than glycerol.

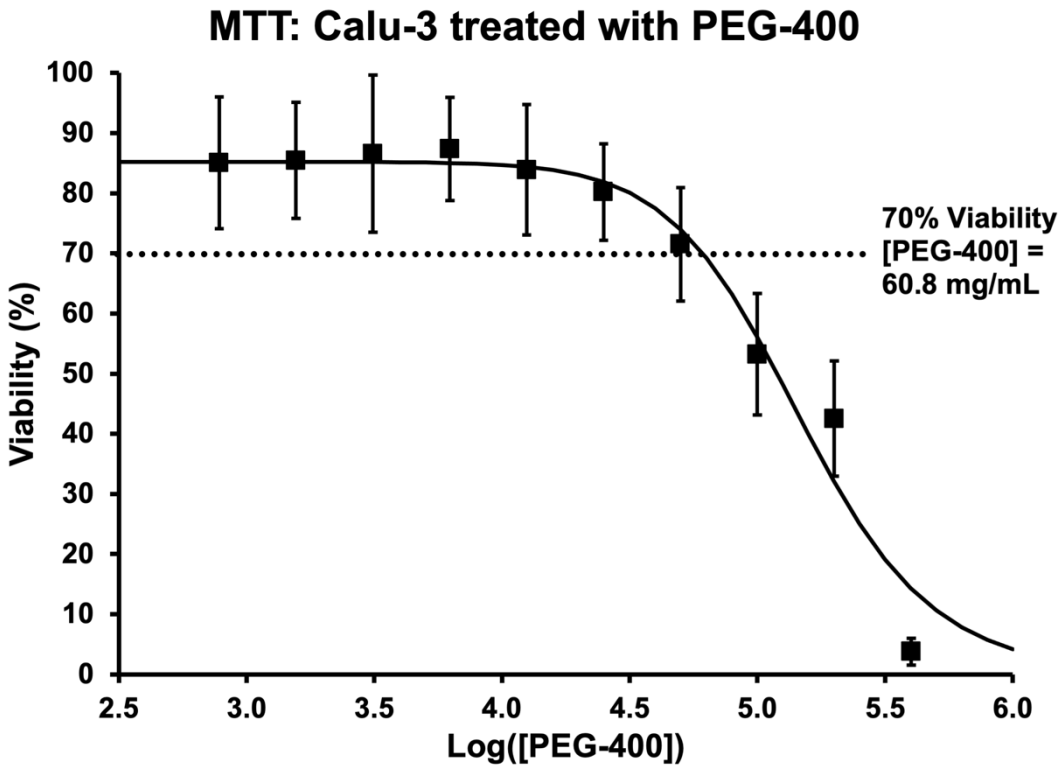

Figure 11. Dose-response curve from MTT results after treating Calu-3 cells with PEG-400.

The dose-response curve in **Figure 11** is the plot of Calu-3 viability vs. log([PEG-400]). The concentration which inhibited 30% of cell growth, corresponding to 70% cell viability, was determined to be 60.8 mg/mL (6.1% *w/v*). These values corresponded to similar results with Caco-2 cells which demonstrated that low molecular weight PEG compounds exhibited moderate cytotoxicity. [98]

Therefore, PEG-400 has potential as a nanoplastic suspension medium. The characteristics which make glycerol ideal are its high viscosity and ability to suspend the nanoplastics, and its solubility in aqueous medium without significant cytotoxicity. This limit presented issues when higher concentrations of nanoplastic are needed to increase the uptake and reduce error associated with uptake values being close to the LOD of each nanoplastic suspension. PEG-400 possesses good solubility in aqueous medium and a slightly lower cytotoxicity, meaning a higher concentration can be exposed to the cells, thus enabling higher concentrations of nanoplastic in future uptake studies. On the other hand, PEG-400 has often been used to coat nanoparticles to increase their solubility in aqueous media and their ability to penetrate cell membranes. [99,100] This characteristic could create misleading uptake results *in vitro*, as an abnormally high number of particles could then cross the cell membrane, in addition to changes to the surface corona induced by PEG-400 coating. Therefore, glycerol should continue to be used as a suspension medium.

5. Conclusion

In summary, nanoplastic suspensions in glycerol of PET–F8BT (0.8%) and PP–F8BT (0.8%) were produced, and PET was found to be polydisperse with a major peak in the colloidal size range. PP had a much sharper and cleaner peak between 0.1 – 1.0 µm. Aggregation remained a problem, with significant volume extending to 100 µm. Calibration curves were measured for both plastic types in PBS and U937 lysate. The results indicated reproducibility of LOD and LOQ values for PET, but very low reproducibility for PP's LOD and LOQ values, brought on by the buoyant and aggregate nature of the PP nanoparticles. Aggregation was shown to increase dramatically for both particle types in cell culture medium. A mass-based fluorescence uptake assay performed with Calu-3 cells using PET–F8BT (5%) and PP–F8BT (5%) indicated no measurable uptake for PP, while PET had inconclusive uptake results, with values of 1.38 ± 0.7 µg/cm^2 (250 µg/mL AD) and 2.84 ± 1.1 µg/cm^2 (500 µg /mL AD). This meant measurable uptake above the LOD, but it was not confirmed whether this stems from experimental errors, since the blank plate measured 0.72 ± 0.4 µg/cm^2 (250 µg/mL AD) and 2.16 ± 0.7 µg/cm^2 (500 µg/mL AD). To identify a different suspension medium, PEG-400 was found to inhibit 30% of cell growth at 6.1% *w/v*, which suggested it could be a possible suspension medium, but this was not further pursued during the scope of this project.

The production method for F8BT-labelled PET and PP suspensions presents a great opportunity for optimization to reduce the fraction of aggregates in suspension by centrifugation and fractionation. Developing a dispersion protocol that preserves colloidal nanoplastic particles while minimizing aggregation by using lower concentrations could significantly enhance the quality of the experiments performed with them, as well as extending the useable life of the glycerol suspensions. F8BT demonstrated ease of labelling and fluorescent stability making it a candidate as a polymer label, and further identification work could deepen the understanding of the polymer structure in nanoplastics, leading optimization of the sensitivity. The work performed in this thesis can hopefully establish further progress towards high-yield, reproducible fluorescent nanoplastic reference material.

List of Figures

List of Tables

References

[1] Chamas A, Moon H, Zheng J, Qiu Y, Tabassum T, Jang JH, et al. Degradation Rates of Plastics in the Environment. ACS Sustainable Chem Eng 2020;8:3494–511. https://doi.org/10.1021/acssuschemeng.9b06635.

[2] Geyer R, Jambeck JR, Law KL. Production, use, and fate of all plastics ever made. Sci Adv 2017;3:e1700782. https://doi.org/10.1126/sciadv.1700782.

[3] Jr J, R G, C W, Tr S, M P, A A, et al. Marine pollution. Plastic waste inputs from land into the ocean. Science (New York, NY) 2015;347. https://doi.org/10.1126/science.1260352.

[4] Barnes DKA, Galgani F, Thompson RC, Barlaz M. Accumulation and fragmentation of plastic debris in global environments. Philos Trans R Soc Lond B Biol Sci 2009;364:1985–98. https://doi.org/10.1098/rstb.2008.0205.

[5] Kumar M, Chen H, Sarsaiya S, Qin S, Liu H, Awasthi MK, et al. Current research trends on micro- and nano-plastics as an emerging threat to global environment: A review. Journal of Hazardous Materials 2021;409:124967. https://doi.org/10.1016/j.jhazmat.2020.124967.

[6] Alimi OS, Farner Budarz J, Hernandez LM, Tufenkji N. Microplastics and Nanoplastics in Aquatic Environments: Aggregation, Deposition, and Enhanced Contaminant Transport. Environ Sci Technol 2018;52:1704–24. https://doi.org/10.1021/acs.est.7b05559.

[7] Gigault J, Halle AT, Baudrimont M, Pascal P-Y, Gauffre F, Phi T-L, et al. Current opinion: What is a nanoplastic? Environ Pollut 2018;235:1030–4. https://doi.org/10.1016/j.envpol.2018.01.024.

[8] ter Halle A, Ghiglione JF. Nanoplastics: A Complex, Polluting Terra Incognita. Environ Sci Technol 2021;55:14466–9. https://doi.org/10.1021/acs.est.1c04142.

[9] ISO/TR 21960:2020(en), Plastics — Environmental aspects — State of knowledge and methodologies n.d. https://www.iso.org/obp/ui/#iso:std:iso:tr:21960:ed-1:v1:en (accessed August 28, 2024).

[10] Chemistry (IUPAC) TIU of P and A. IUPAC - colloidal (C01172) n.d. https://doi.org/10.1351/goldbook.C01172.

[11] B. Paul M, Stock V, Cara-Carmona J, Lisicki E, Shopova S, Fessard V, et al. Micro- and nanoplastics – current state of knowledge with the focus on oral uptake and toxicity. Nanoscale Advances 2020;2:4350–67. https://doi.org/10.1039/D0NA00539H.

[12] Allen S, Allen D, Karbalaei S, Maselli V, Walker TR. Micro(nano)plastics sources, fate, and effects: What we know after ten years of research. Journal of Hazardous Materials Advances 2022;6:100057. https://doi.org/10.1016/j.hazadv.2022.100057.

[13] Ali N, Katsouli J, Marczylo EL, Gant TW, Wright S, Serna JB de la. The potential impacts of micro-and-nano plastics on various organ systems in humans. eBioMedicine 2024;99. https://doi.org/10.1016/j.ebiom.2023.104901.

[14] Jenner LC, Rotchell JM, Bennett RT, Cowen M, Tentzeris V, Sadofsky LR. Detection of microplastics in human lung tissue using μFTIR spectroscopy. Science of The Total Environment 2022;831:154907. https://doi.org/10.1016/j.scitotenv.2022.154907.

[15] Correia AW, Pope CA, Dockery DW, Wang Y, Ezzati M, Dominici F. The Effect of Air Pollution Control on Life Expectancy in the United States: An Analysis of 545 US counties for the period 2000 to 2007. Epidemiology 2013;24:23–31. https://doi.org/10.1097/EDE.0b013e3182770237.

[16] Xing Y-F, Xu Y-H, Shi M-H, Lian Y-X. The impact of PM2.5 on the human respiratory system. Journal of Thoracic Disease 2016;8. https://doi.org/10.3978/j.issn.2072-1439.2016.01.19.
[17] Xu M, Halimu G, Zhang Q, Song Y, Fu X, Li Y, et al. Internalization and toxicity: A preliminary study of effects of nanoplastic particles on human lung epithelial cell. Science of the Total Environment 2019;694. https://doi.org/10.1016/j.scitotenv.2019.133794.
[18] Woo J-H, Seo HJ, Lee J-Y, Lee I, Jeon K, Kim B, et al. Polypropylene nanoplastic exposure leads to lung inflammation through p38-mediated NF-κB pathway due to mitochondrial damage. Particle and Fibre Toxicology 2023;20:2. https://doi.org/10.1186/s12989-022-00512-8.
[19] Kirchsteiger B, Materić D, Happenhofer F, Holzinger R, Kasper-Giebl A. Fine micro- and nanoplastics particles (PM2.5) in urban air and their relation to polycyclic aromatic hydrocarbons. Atmospheric Environment 2023;301:119670. https://doi.org/10.1016/j.atmosenv.2023.119670.
[20] de Ruijter VN, Redondo-Hasselerharm PE, Gouin T, Koelmans AA. Quality Criteria for Microplastic Effect Studies in the Context of Risk Assessment: A Critical Review. Environ Sci Technol 2020;54:11692–705. https://doi.org/10.1021/acs.est.0c03057.
[21] Hartmann NB, Hüffer T, Thompson RC, Hassellöv M, Verschoor A, Daugaard AE, et al. Are We Speaking the Same Language? Recommendations for a Definition and Categorization Framework for Plastic Debris. Environ Sci Technol 2019;53:1039–47. https://doi.org/10.1021/acs.est.8b05297.
[22] Hildebrandt J, Thünemann AF. Aqueous Dispersions of Polypropylene: Toward Reference Materials for Characterizing Nanoplastics. Macromolecular Rapid Communications 2023;44:2200874. https://doi.org/10.1002/marc.202200874.
[23] Teeguarden JG, Hinderliter PM, Orr G, Thrall BD, Pounds JG. Particokinetics In Vitro: Dosimetry Considerations for In Vitro Nanoparticle Toxicity Assessments. Toxicological Sciences 2007;95:300–12. https://doi.org/10.1093/toxsci/kfl165.
[24] Ahmad Khanbeigi R, Kumar A, Sadouki F, Lorenz C, Forbes B, Dailey LA, et al. The delivered dose: Applying particokinetics to in vitro investigations of nanoparticle internalization by macrophages. Journal of Controlled Release 2012;162:259–66. https://doi.org/10.1016/j.jconrel.2012.07.019.
[25] Limbach LK, Li Y, Grass RN, Brunner TJ, Hintermann MA, Muller M, et al. Oxide Nanoparticle Uptake in Human Lung Fibroblasts: Effects of Particle Size, Agglomeration, and Diffusion at Low Concentrations. Environ Sci Technol 2005;39:9370–6. https://doi.org/10.1021/es051043o.
[26] Zhu M, Perrett S, Nie G. Understanding the Particokinetics of Engineered Nanomaterials for Safe and Effective Therapeutic Applications. Small 2013;9:1619–34. https://doi.org/10.1002/smll.201201630.
[27] Brown JS, Wilson WE, Grant LD. Dosimetric comparisons of particle deposition and retention in rats and humans. Inhal Toxicol 2005;17:355–85. https://doi.org/10.1080/08958370590929475.
[28] Schroeter JD, Kimbell JS, Bonner AM, Roberts KC, Andersen ME, Dorman DC. Incorporation of Tissue Reaction Kinetics in a Computational Fluid Dynamics Model for Nasal Extraction of Inhaled Hydrogen Sulfide in Rats. Toxicological Sciences 2006;90:198–207. https://doi.org/10.1093/toxsci/kfj072.
[29] DeLoid GM, Cohen JM, Pyrgiotakis G, Pirela SV, Pal A, Liu J, et al. Advanced computational modeling for in vitro nanomaterial dosimetry. Particle and Fibre Toxicology 2015;12:32. https://doi.org/10.1186/s12989-015-0109-1.

[30] Paget V, Dekali S, Kortulewski T, Grall R, Gamez C, Blazy K, et al. Specific Uptake and Genotoxicity Induced by Polystyrene Nanobeads with Distinct Surface Chemistry on Human Lung Epithelial Cells and Macrophages. PLOS ONE 2015;10:e0123297. https://doi.org/10.1371/journal.pone.0123297.
[31] Monopoli MP, Åberg C, Salvati A, Dawson KA. Biomolecular coronas provide the biological identity of nanosized materials. Nature Nanotech 2012;7:779–86. https://doi.org/10.1038/nnano.2012.207.
[32] Ahmad Khanbeigi R, Abelha TF, Woods A, Rastoin O, Harvey RD, Jones M-C, et al. Surface Chemistry of Photoluminescent F8BT Conjugated Polymer Nanoparticles Determines Protein Corona Formation and Internalization by Phagocytic Cells. Biomacromolecules 2015;16:733–42. https://doi.org/10.1021/bm501649y.
[33] Schvartz M, Saudrais F, Devineau S, Chédin S, Jamme F, Leroy J, et al. Role of the Protein Corona in the Colloidal Behavior of Microplastics. Langmuir 2023;39:4291–303. https://doi.org/10.1021/acs.langmuir.2c03237.
[34] Mason M, Weaver W. The Settling of Small Particles in a Fluid. Phys Rev 1924;23:412–26. https://doi.org/10.1103/PhysRev.23.412.
[35] Hinderliter PM, Minard KR, Orr G, Chrisler WB, Thrall BD, Pounds JG, et al. ISDD: A computational model of particle sedimentation, diffusion and target cell dosimetry for in vitro toxicity studies. Particle and Fibre Toxicology 2010;7:36. https://doi.org/10.1186/1743-8977-7-36.
[36] DeLoid GM, Cohen JM, Pyrgiotakis G, Demokritou P. An integrated dispersion preparation, characterization and in vitro dosimetry methodology for engineered nanomaterials. Nat Protoc 2017;12:355–71. https://doi.org/10.1038/nprot.2016.172.
[37] Kik K, Bukowska B, Sicińska P. Polystyrene nanoparticles: Sources, occurrence in the environment, distribution in tissues, accumulation and toxicity to various organisms. Environmental Pollution 2020;262:114297. https://doi.org/10.1016/j.envpol.2020.114297.
[38] Alsabri A, Tahir F, Al-Ghamdi SG. Environmental impacts of polypropylene (PP) production and prospects of its recycling in the GCC region. Materials Today: Proceedings 2022;56:2245–51. https://doi.org/10.1016/j.matpr.2021.11.574.
[39] Consolati G, Quasso F. An experimental study of the occupied volume in polyethylene terephthalate. The Journal of Chemical Physics 2001;114:2825–9. https://doi.org/10.1063/1.1338980.
[40] E T, M T, K L, T V, E L. Toxicity of ethanol in low concentrations. Experimental evaluation in cell culture. Acta Radiologica (Stockholm, Sweden : 1987) 1996;37. https://doi.org/10.1177/02841851960373P296.
[41] van Uunen D, Kloukinioti M, Kooter IM, Höppener EM, Yoe LEA, Brunner AM, et al. Suspension of micro- and nanoplastic test materials: Liquid compatibility, (bio)surfactants, toxicity and environmental relevance. Environmental Pollution 2024;356:124306. https://doi.org/10.1016/j.envpol.2024.124306.
[42] Parveen R, Ullah S, Sgarbi R, Tremiliosi-Filho G. One-pot ligand-free synthesis of gold nanoparticles: The role of glycerol as reducing-cum-stabilizing agent. Colloids and Surfaces A: Physicochemical and Engineering Aspects 2019;565:162–71. https://doi.org/10.1016/j.colsurfa.2019.01.005.
[43] Lee WS, Kim H, Sim Y, Kang T, Jeong J. Fluorescent Polypropylene Nanoplastics for Studying Uptake, Biodistribution, and Excretion in Zebrafish Embryos. ACS Omega 2022;7:2467–73. https://doi.org/10.1021/acsomega.1c06779.

[44] Lu W, Yuan Z, Zhao Y, Zhang H, Zhang H, Li X. Porous membranes in secondary battery technologies. Chem Soc Rev 2017;46:2199–236. https://doi.org/10.1039/C6CS00823B.
[45] LOEB S, SOURIRAJAN S. Sea Water Demineralization by Means of an Osmotic Membrane. Saline Water Conversion—II, vol. 38, AMERICAN CHEMICAL SOCIETY; 1963, p. 117–32. https://doi.org/10.1021/ba-1963-0038.ch009.
[46] Young T-H, Chen L-W. Pore formation mechanism of membranes from phase inversion process. Desalination 1995;103:233–47. https://doi.org/10.1016/0011-9164(95)00076-3.
[47] Achilias DS, Giannoulis A, Papageorgiou GZ. Recycling of polymers from plastic packaging materials using the dissolution–reprecipitation technique. Polym Bull 2009;63:449–65. https://doi.org/10.1007/s00289-009-0104-5.
[48] Rodríguez-Hernández AG, Muñoz-Tabares JA, Aguilar-Guzmán JC, Vazquez-Duhalt R. A novel and simple method for polyethylene terephthalate (PET) nanoparticle production. Environ Sci: Nano 2019;6:2031–6. https://doi.org/10.1039/C9EN00365G.
[49] M. Johnson L, B. Mecham J, Archana Krovi S, Caffaro MMM, Aravamudhan S, L. Kovach A, et al. Fabrication of polyethylene terephthalate (PET) nanoparticles with fluorescent tracers for studies in mammalian cells. Nanoscale Advances 2021;3:339–46. https://doi.org/10.1039/D0NA00888E.
[50] Rosiuk V, Runser A, Klymchenko A, Reisch A. Controlling Size and Fluorescence of Dye-Loaded Polymer Nanoparticles through Polymer Design. Langmuir 2019;35:7009–17. https://doi.org/10.1021/acs.langmuir.9b00721.
[51] Schwaferts C, Niessner R, Elsner M, Ivleva NP. Methods for the analysis of submicrometer- and nanoplastic particles in the environment. TrAC Trends in Analytical Chemistry 2019;112:52–65. https://doi.org/10.1016/j.trac.2018.12.014.
[52] Mamada M, Komatsu R, Adachi C. F8BT Oligomers for Organic Solid-State Lasers. ACS Appl Mater Interfaces 2020;12:28383–91. https://doi.org/10.1021/acsami.0c05449.
[53] Borges BG, Veiga AG, Gioti M, Laskarakis A, Tzounis L, Logothetidis S, et al. Surface, interface and electronic properties of F8:F8BT polymeric thin films used for organic light-emitting diode applications. Polymer International 2018;67:691–9. https://doi.org/10.1002/pi.5552.
[54] González Sierra J, Martin-Merinero A, Álvarez-Conde J, Iglesias Vázquez S, Cabanillas-González J, Wannemacher R. High Q Ultra-Low Threshold Lasing in Conjugated Polymer Blend Microspheres Promoted by FRET. Advanced Optical Materials 2024;12:2400161. https://doi.org/10.1002/adom.202400161.
[55] Raval JB, Kailasa SK, Mehta VN. Chapter 3 - An overview of optical, physical, biological, and catalytic properties of carbon dots. In: Kailasa SK, Hussain CM, editors. Carbon Dots in Analytical Chemistry, Elsevier; 2023, p. 31–41. https://doi.org/10.1016/B978-0-323-98350-1.00026-8.
[56] Abelha TF, Phillips TW, Bannock JH, Nightingale AM, Dreiss CA, Kemal E, et al. Bright conjugated polymer nanoparticles containing a biodegradable shell produced at high yields and with tuneable optical properties by a scalable microfluidic device. Nanoscale 2017;9:2009–19. https://doi.org/10.1039/C6NR09162H.
[57] Sommer ME, Elgeti M, Hildebrand PW, Szczepek M, Hofmann KP, Scheerer P. Chapter Twenty-Six - Structure-Based Biophysical Analysis of the Interaction of Rhodopsin with G Protein and Arrestin. In: Shukla AK, editor. Methods in Enzymology, vol. 556, Academic Press; 2015, p. 563–608. https://doi.org/10.1016/bs.mie.2014.12.014.

[58] Peng H-S, Chiu DT. Soft fluorescent nanomaterials for biological and biomedical imaging. Chem Soc Rev 2015;44:4699–722. https://doi.org/10.1039/c4cs00294f.
[59] Visaveliya NR, Köhler JM. Softness Meets with Brightness: Dye-Doped Multifunctional Fluorescent Polymer Particles via Microfluidics for Labeling. Advanced Optical Materials 2021;9:2002219. https://doi.org/10.1002/adom.202002219.
[60] Visaveliya N, Hoffmann C, Groß A, Täuscher E, Ritter U, Koehler JM. Micro-flow assisted synthesis of fluorescent polymer nanoparticles with tuned size and surface properties. Nanotechnology Reviews 2016;5:259–72. https://doi.org/10.1515/ntrev-2015-0061.
[61] Harcourt JL, Caidi H, Anderson LJ, Haynes LM. Evaluation of the Calu-3 cell line as a model of in vitro respiratory syncytial virus infection. J Virol Methods 2011;174:144–9. https://doi.org/10.1016/j.jviromet.2011.03.027.
[62] Chanput W, Peters V, Wichers H. THP-1 and U937 Cells. In: Verhoeckx K, Cotter P, López-Expósito I, Kleiveland C, Lea T, Mackie A, et al., editors. The Impact of Food Bioactives on Health: in vitro and ex vivo models, Cham: Springer International Publishing; 2015, p. 147–59. https://doi.org/10.1007/978-3-319-16104-4_14.
[63] Prietl B, Meindl C, Roblegg E, Pieber TR, Lanzer G, Fröhlich E. Nano-sized and micro-sized polystyrene particles affect phagocyte function. Cell Biol Toxicol 2014;30:1–16. https://doi.org/10.1007/s10565-013-9265-y.
[64] Pelegrini K, Pereira TCB, Maraschin TG, Teodoro LDS, Basso NRDS, De Galland GLB, et al. Micro- and nanoplastic toxicity: A review on size, type, source, and test-organism implications. Science of The Total Environment 2023;878:162954. https://doi.org/10.1016/j.scitotenv.2023.162954.
[65] Oberdörster G. Nanotoxicology: in Vitro–in Vivo Dosimetry. Environ Health Perspect 2012;120:a13. https://doi.org/10.1289/ehp.1104320.
[66] Langevin D, Raspaud E, Mariot S, Knyazev A, Stocco A, Salonen A, et al. Towards reproducible measurement of nanoparticle size using dynamic light scattering: Important controls and considerations. NanoImpact 2018;10:161–7. https://doi.org/10.1016/j.impact.2018.04.002.
[67] Li J, Huang F, Zhang G, Zhang Z, Zhang X. Separation and flow cytometry analysis of microplastics and nanoplastics. Front Chem 2023;11:1201734. https://doi.org/10.3389/fchem.2023.1201734.
[68] Huang S, Huang X, Bi R, Guo Q, Yu X, Zeng Q, et al. Detection and Analysis of Microplastics in Human Sputum. Environ Sci Technol 2022;56:2476–86. https://doi.org/10.1021/acs.est.1c03859.
[69] Adhikari S, Kelkar V, Kumar R, Halden RU. Methods and challenges in the detection of microplastics and nanoplastics: a mini-review. Polymer International 2022;71:543–51. https://doi.org/10.1002/pi.6348.
[70] Botha J, Pugsley HR, Handberg A. Conventional, High-Resolution and Imaging Flow Cytometry: Benchmarking Performance in Characterisation of Extracellular Vesicles. Biomedicines 2021;9:124. https://doi.org/10.3390/biomedicines9020124.
[71] Stetefeld J, McKenna SA, Patel TR. Dynamic light scattering: a practical guide and applications in biomedical sciences. Biophys Rev 2016;8:409–27. https://doi.org/10.1007/s12551-016-0218-6.
[72] Mie G. Beiträge zur Optik trüber Medien, speziell kolloidaler Metallösungen. Annalen Der Physik 1908;330:377–445. https://doi.org/10.1002/andp.19083300302.
[73] Sun Y. Different Particle Size Information Obtained From Static and Dynamic Laser Light Scattering 2004.

[74] Hodgson RJW. Genetic Algorithm Approach to the Determination of Particle Size Distributions from Static Light-Scattering Data. Journal of Colloid and Interface Science 2001;240:412–8. https://doi.org/10.1006/jcis.2001.7652.
[75] Hassan PA, Rana S, Verma G. Making Sense of Brownian Motion: Colloid Characterization by Dynamic Light Scattering. Langmuir 2015;31:3–12. https://doi.org/10.1021/la501789z.
[76] Uhrovčík J. Strategy for determination of LOD and LOQ values – Some basic aspects. Talanta 2014;119:178–80. https://doi.org/10.1016/j.talanta.2013.10.061.
[77] Cheimarios N, Pem B, Tsoumanis A, Ilić K, Vrček IV, Melagraki G, et al. An In Vitro Dosimetry Tool for the Numerical Transport Modeling of Engineered Nanomaterials Powered by the Enalos RiskGONE Cloud Platform. Nanomaterials (Basel) 2022;12:3935. https://doi.org/10.3390/nano12223935.
[78] Riss T, Moravec R, Niles A. Structures of MTT and colored formazan product. Cell Viability Assays, n.d.
[79] Berridge MV, Herst PM, Tan AS. Tetrazolium dyes as tools in cell biology: new insights into their cellular reduction. Biotechnol Annu Rev 2005;11:127–52. https://doi.org/10.1016/S1387-2656(05)11004-7.
[80] Ghasemi M, Turnbull T, Sebastian S, Kempson I. The MTT Assay: Utility, Limitations, Pitfalls, and Interpretation in Bulk and Single-Cell Analysis. Int J Mol Sci 2021;22:12827. https://doi.org/10.3390/ijms222312827.
[81] Scherließ R. The MTT assay as tool to evaluate and compare excipient toxicity *in vitro* on respiratory epithelial cells. International Journal of Pharmaceutics 2011;411:98–105. https://doi.org/10.1016/j.ijpharm.2011.03.053.
[82] Zhang Y, Ying L, Wang Z, Wang Y, Xu Q, Li C. Unexpected hydrophobic to hydrophilic transition of PET fabric treated in a deep eutectic solvent of choline chloride and oxalic acid. Polymer 2021;234:124246. https://doi.org/10.1016/j.polymer.2021.124246.
[83] Dubey V, Daschakraborty S. Influence of glycerol on the cooling effect of pair hydrophobicity in water: relevance to proteins' stabilization at low temperature. Phys Chem Chem Phys 2019;21:800–12. https://doi.org/10.1039/C8CP06513F.
[84] Lee J-H, Gomez IJ, Sitterle VB, Meredith JC. Dye-labeled polystyrene latex microspheres prepared via a combined swelling-diffusion technique. J Colloid Interface Sci 2011;363:137–44. https://doi.org/10.1016/j.jcis.2011.07.047.
[85] Aguilar-Guzmán JC, Bejtka K, Fontana M, Valsami-Jones E, Villezcas AM, Vazquez-Duhalt R, et al. Polyethylene terephthalate nanoparticles effect on RAW 264.7 macrophage cells. Microplastics and Nanoplastics 2022;2:9. https://doi.org/10.1186/s43591-022-00027-1.
[86] Lee C-H, Fang JK-H. Effects of temperature and particle concentration on aggregation of nanoplastics in freshwater and seawater. Science of The Total Environment 2022;817:152562. https://doi.org/10.1016/j.scitotenv.2021.152562.
[87] Chen H, Hu Q, Li W, Cai X, Mao L, Li R. Approaches to Nanoparticle Labeling: A Review of Fluorescent, Radiological, and Metallic Techniques. Environ Health 2023;1:75–89. https://doi.org/10.1021/envhealth.3c00034.
[88] Zulbeari N, Holm R. Wet bead milling by dual centrifugation – An approach to obtain reproducible and differentiable suspensions. International Journal of Pharmaceutics 2023;646:123455. https://doi.org/10.1016/j.ijpharm.2023.123455.
[89] Ferreira AGM, Egas APV, Fonseca IMA, Costa AC, Abreu DC, Lobo LQ. The viscosity of glycerol. The Journal of Chemical Thermodynamics 2017;113:162–82. https://doi.org/10.1016/j.jct.2017.05.042.

[90] Kestin J, Sokolov M, Wakeham WA. Viscosity of liquid water in the range −8 °C to 150 °C. Journal of Physical and Chemical Reference Data 1978;7:941–8. https://doi.org/10.1063/1.555581.
[91] Beysens D. Brownian motion in strongly fluctuating liquid. Thermodynamics of Interfaces and Fluid Mechanics 2019;3:1–8.
[92] Schubert J, Chanana M. Coating Matters: Review on Colloidal Stability of Nanoparticles with Biocompatible Coatings in Biological Media, Living Cells and Organisms. Curr Med Chem 2019;25:4556–86. https://doi.org/10.2174/0929867325666180601101859.
[93] Moore TL, Rodriguez-Lorenzo L, Hirsch V, Balog S, Urban D, Jud C, et al. Nanoparticle colloidal stability in cell culture media and impact on cellular interactions. Chem Soc Rev 2015;44:6287–305. https://doi.org/10.1039/c4cs00487f.
[94] Dewald I, Isakin O, Schubert J, Kraus T, Chanana M. Protein Identity and Environmental Parameters Determine the Final Physicochemical Properties of Protein-Coated Metal Nanoparticles. J Phys Chem C 2015;119:25482–92. https://doi.org/10.1021/acs.jpcc.5b06266.
[95] Watson CY, DeLoid GM, Pal A, Demokritou P. Buoyant Nanoparticles: Implications for Nano-Biointeractions in Cellular Studies. Small 2016;12:3172–80. https://doi.org/10.1002/smll.201600314.
[96] Busch M, Kämpfer AAM, Schins RPF. An inverted in vitro triple culture model of the healthy and inflamed intestine: Adverse effects of polyethylene particles. Chemosphere 2021;284:131345. https://doi.org/10.1016/j.chemosphere.2021.131345.
[97] Ihekwereme C, Esimone C, Shao D, Agu RU. Preliminary Studies on Validation of Calu-3 Cell Line as a Model for Screening Respiratory Mucosa Irritation and Toxicity. Pharmaceutics 2014;6:268–80. https://doi.org/10.3390/pharmaceutics6020268.
[98] Pham Le Khanh H, Nemes D, Rusznyák Á, Ujhelyi Z, Fehér P, Fenyvesi F, et al. Comparative Investigation of Cellular Effects of Polyethylene Glycol (PEG) Derivatives. Polymers (Basel) 2022;14:279. https://doi.org/10.3390/polym14020279.
[99] Zomorodian K, Veisi H, Mousavi SM, Ataabadi MS, Yazdanpanah S, Bagheri J, et al. Modified magnetic nanoparticles by PEG-400-immobilized Ag nanoparticles (Fe3O4@PEG–Ag) as a core/shell nanocomposite and evaluation of its antimicrobial activity. Int J Nanomedicine 2018;13:3965–73. https://doi.org/10.2147/IJN.S161002.
[100] Chandra Mohanta S, Saha A, Sujatha Devi P. PEGylated Iron Oxide Nanoparticles for pH Responsive Drug Delivery Application. Materials Today: Proceedings 2018;5:9715–25. https://doi.org/10.1016/j.matpr.2017.10.158.

Appendix

Abstract (Deutsch)

Kunststoffpartikel wurden weltweit in der Umwelt nachgewiesen, und in letzter Zeit wurden kleinere Partikel, so genannte Nanokunststoffe, in Luftproben nachgewiesen, die bis in entlegene alpine Gebiete reichten. Die Auswirkungen von Nanokunststoffen auf die menschliche Gesundheit sind immer noch unklar, so dass weitere Forschungsarbeiten erforderlich sind, um ihre potenziellen toxikologischen Auswirkungen und die Folgen für die menschliche Exposition zu verstehen. Nanokunststoffe sind oft inhomogen und variieren in Größe, Oberflächenchemie und Struktur. Dies führt zu nicht vergleichbaren Dosiswerten zwischen den Studien. Um die biologischen Auswirkungen von Nanokunststoffen besser zu verstehen, müssen neben der Verbesserung der Nachweisverfahren auch zuverlässigere Referenzmaterialien hergestellt werden. In dieser Studie wurden mit Poly(9,9-dioctylfluoren-alt-benzothiadiazol) (F8BT) markierte fluoreszierende Polypropylen (PP)- und Polyethylenterephthalat (PET)-Nanopartikel mit unterschiedlichen Prozentsätzen der Farbstoffbeladung (0,8 % und 5 %) durch Nanopräzipitation hergestellt und die Größenverteilungen durch statische Lichtstreuung (SLS) gemessen. PP-F8BT (0,8 %) und PET-F8BT (0,8 %) wurden im Bereich von 0,1 – 1,0 µm hergestellt, aber die Aggregation führte zur Bildung großer Partikel, sowohl in Glycerin als auch in biorelevanten Mediumssuspensionen. Die Nachweisgrenze (LOD) von PET-F8BT (0,8%) war in Dulbeccos phosphatgepufferter Kochsalzlösung (PBS) um das 10-fache und in makrophagenähnlich differenziertem, pro-monozytärem humanem myeloischem Leukämie U937 Lysat und um das 5-fache niedriger als bei PP-F8BT (0,8%). Die theoretischen Werte der abgegebenen Dosis wurden mit zwei Berechnungsmethoden berechnet, der *in vitro* Sedimentations-, Diffusions- und Dosimetrie (ISDD) und der RiskGone *in vitro* Dosimetrie. Auf der Grundlage der von den Berechnungsmodellen vorhergesagten Konzentrationen wurden Calu-3-Lungenepithelzellen des Menschen mit PP-F8BT (5 %) und PET-F8BT (5 %) Glycerinsuspensionen behandelt, und die zelluläre Aufnahme wurde durch Fluoreszenzdetektion auf Massenbasis bewertet. Die zelluläre Dosis wurde für PET-F8BT (5%) mit 250 µg/mL = 1,38 ± 0,7 µg/cm^2 und 500 µg/mL = 2,84 ± 1,1 µg/cm^2 gemessen, aber das Hintergrundsignal war fast genauso hoch. PP wies keine messbare Aufnahme auf.